7 Crude Oil Environment

7.1 Crude Oil Chemistry Analysis

Compared to conventional crude oil, bitumen and diluted bitumen (dilbit) contain elevated concentrations of sulfur, naphthenic acids (measured by total acid number, TAN), iron species, and asphaltenes. [28] [29]

The industry also distinguishes bitumen from conventional crude oil. For instance, Bruce (2005) described bitumen in a presentation for Jacobs Canada Inc. at a Canadian Heavy Oil Association Technical Luncheon as having a complex chemistry characterized by significant amounts of aromatic and asphaltene compounds, high levels of sulfur, nitrogen, metals, and organic acids [30]. According to the Oil Sands Review glossary, bitumen is defined as a "naturally occurring, viscous mixture of hydrocarbons that contains high levels of sulfur and nitrogen compounds" (www.oilsandsreview.com).

7.1.1 Objectives

The intent is to characterize the potential contribution of the total bitumen system to electrochemical reactions in the presence of tiny amounts of water in the presence of sulfur and acids. It is essential to note that only petroleum having properties that conform to agreed specifications for petroleum quality between South Bow and shippers will be permitted to be accepted and transported on the pipeline system, where specifically there is a requirement that the basic sediment and water shall not exceed 0.5% of volume. The intent for the rest of this section is to review all of the information provided regarding dilbit compositions. A compositional model will be created, and OLI Studio thermodynamic chemistry software will be used to simulate chemical reactions that may occur and identify any conditions that could contribute to hydrogen production. The emphasis will be on the potential for the composition to produce hydrogen sulfide (H_2S). It is known that H_2S, in conjunction with an aqueous environment, can provide a source of hydrogen atoms that contribute to embrittling conditions.

7.1.2 Crude Chemical Composition

This section will review the compositional components that could contribute to increased and unexpected chemical reactivity. We will review each component and how it will be used in the simulation. The focus will be on the aspects of the composition that ultimately are used in the OLI Studio Thermodynamic Simulations.

Sulfur

Heavy oil crude is considered unconventional. Several characteristics lead to the designation. For this report, we are primarily concerned with the sulfur content in the diluted bitumen, which is between 3-5%.

Table 15 shows one of the analyses given for the crude in the pipeline. As expected, the sulfur content is between 3-5%. Literature and other sources do not provide much additional information regarding the exact form of sulfur. It would be inappropriate to assume that all of the sulfur at those concentrations is in a particular form, such as elemental sulfur, mercaptans, thiophenes, and iron sulfide. [31]

The conservative approach is to consider the "reactivity" of whatever form is present. In other words, how easily can the "form" of sulfur convert to H_2S or acid in the presence of trace water and naphthenic acid? For the OLI simulation, it was assumed that some of the sulfur exists as colloidal, elemental sulfur and as a simple thiol compound (mercaptan). These example forms were input into OLI and analyzed in the context of other factors that may facilitate the reactions of sulfur. One of the reactions possible with elemental, colloidal sulfur is shown in Equation 10.

What should also be noted is that this reaction is acid-catalyzed, in that it is kinetically faster the more acidic the aqueous phase is. In addition, in the presence of excess water, the equilibrium will shift more to the right as the sulfur dioxide is converted to sulfurous acid. Here, the water is assumed to be around 0.2 to 0.5%. Sulfur dioxide dissolved in water forms sulfurous acid, which will significantly lower the pH than will be expected from naphthenic acids. In the OLI Studio simulations, when H_2S is formed, the model predicts a pH range of 1.3 to 2.6 in the water droplet.

$$3S_{(s)} + 2H_2O \rightarrow 2H_2S + SO_2 \tag{10}$$

Table 15: Example of crude sample showing high sulfur content

CLKB319Y	Whole Crude
Cut volume, %	100.0
API Gravity	20.1
Specific Gravity (60/60),	0.934
Carbon, wt %	84.5
Hydrogen, wt %	12.1
Pour point, F	(27.4)
Neutralization number (TAN, MG/GM	1.320
Sulfur, wt %	3.750
Viscosity at 20C/68F, cSt	307.6
Viscosity at 40C/104F, cSt	88.8
Viscosity at 50C/122F, cSt	54.
Mercaptan sulfure, ppm	84.1
Nitrogen, ppm	3,171.5
CCR, wt %	10.3
n-Heptane Insoluables (C7 Asphaltenes), wt %	7.8
Nickel, ppm	55.9
Vanadium, ppm	148.3
Calcium, ppm	1.2
Reid Vapor Pressure (RVP) Whole Crude, psi	4.6
Hyrdogen Sulfide (dissolved), ppm	-
Salt Content, ptb	8.8

CLKB319Y	Whole Crude
Paraffins, vol %	21.2
Naphthenes, vol %	23.7

Total Acid Number

Naphthenic acids are a group of organic acids measured in terms of a total acid number (TAN), which is obtained by titration of the oil with KOH. TAN numbers, therefore, have units of milligrams of potassium hydroxide per gram (mg KOH/g).

Our consideration of Naphthenic acid is how the acid group can influence the pH inside the water droplet and stabilize an emulsified water particle. In this scenario, it is a Bronstad proton donor and can be modeled against pipeline conditions. The crude in the pipeline had a TAN of 2.48. This high of a TAN will stabilize a high amount of water in the oil. It also creates a low pH within dispersed emulsified water droplets. The pH can range from 5 to 7 due to the presence of naphthenic acid, which can create a reactive condition for the sulfur present. To simulate this in OLI, we used a large organic acid with a similar molecular weight and pKa to what might be expected for naphthenic acid.

Figure 62 illustrates the consistent increase in TAN numbers as the percentage of crude makeup in the pipeline increased from 2010 to 2025. This would likely correlate to a lower pH of emulsified water and a higher amount of trapped water in the flowing crude. It is factual that these naphthenic acid moieties can provide protons and create acidic conditions in the presence of an aqueous phase, simply by considering the actual measurement. This indicates the availability of protons to create acidic conditions sufficient to catalyze the reactions referenced in this work.

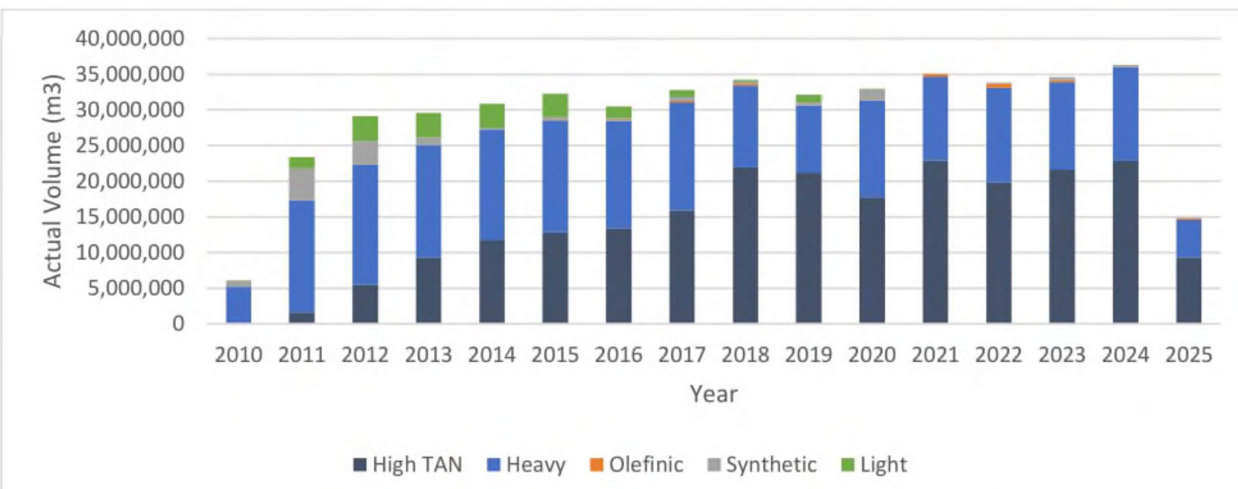

Figure 62: TAN over time of the crude in the Keystone pipeline

Water Content

The specification for water is maintained at a very low level. However, it could be as high as 0.5% of volume or 5,000 ppm. Approximately 2,000 ppm (0.2%) was used for the OLI simulations. Typically, water is viewed as required for corrosion. In other words, a continuous water phase must form and remain in contact with the steel pipeline for corrosion to occur. Considering that, an appropriate conclusion is that the water is not in sufficient concentration to be an issue. However, that is not the corrosion mechanism being evaluated in this analysis. It is considered that if adequate water is present above the solubility limit in the dilbit, the water exists in the form of small droplets or particles that are fully suspended in the oil. Inside this droplet, in the presence of naphthenic acid and sufficiently reactive sulfur, chemical reactions can occur that form H_2S. These droplets act like tiny "chemical reactors" capable of producing H_2S. The question is how much can form, which is what this analysis aims to predict based on thermodynamic modeling using OLI Studio.

At a water content of 0.2% of volume, there was the potential to create H_2S in the presence of sulfur. For droplets of water to form, the water solubility at the temperature conditions of the pipeline must be lower than the actual measured amount in the oil. High TAN and asphaltene oil can create stable conditions for acidic droplets and H_2S production at a water content of 0.2%. We also found that this was more likely to occur at low temperatures, due to the low solubility of water in the dilbit. To reiterate, the water must exist as a distinct phase within the oil for the H_2S-producing reactions to occur.

Iron Content

Iron is present at higher concentrations in Alberta Dilbit [31]. There are two predominant sources: inherent iron in the bitumen and iron introduced through corrosion and erosion from upstream piping and processing equipment. For heavy crudes or bitumen, iron can be present at concentrations ranging from 120-500 ppm [32]. Throughout the life of the crude, from mining to entering the pipeline, it can react with H_2S and form iron sulfide. Iron sulfide can react with existing naphthenic acids to form hydrogen sulfide (H_2S), as shown in Equation 11. OLI predicts a pH as low as 2.0 as a result of the reaction in Equation 11.

$$FeS + 2H^{+} \rightarrow Fe^{+2} + H_2S \qquad (11)$$

Drag Reduction Additive (DRA)

A DRA product is constantly injected at several points along the pipeline. DRA products are essentially insoluble aliphatic polymers dispersed in water. The entire formation contains 40-60% water, with a small amount of glycol and surfactant. The polymer is not soluble in water, which is why it is dispersed in water. In addition, in its pure state, it is highly viscous.

DRA polymers are completely inert. They function to dissolve in the oil phase and elongate, which reduces eddy currents in the oil and lowers pipe friction due to turbulence. There are no known mechanisms by which DRA polymers will cause corrosion.

The second component to discuss is the 40-60% water. The provided information states that the DRA is injected at 3 ppm, which means that it adds approximately 2 ppm of water, which calculates to 0.0002%. The oil contains approximately 1,000-2,000 ppm water or 0.1-0.2%. It is unlikely that this additional water contributes significantly to conditions more likely to cause corrosion.

Summary:

- DRA polymers are chemically inert and do not participate in corrosion mechanisms.

- The additional water introduced via DRA injection is statistically and chemically insignificant in altering corrosion dynamics.

OLI Studio Thermodynamic Reaction Simulation

The objective of this work is to assess if there is a thermodynamic case to predict the production of H_2S in the diluted bitumen stream from the combined chemical reactivity of the components discussed. First, to set up the model, we needed to input meaningful compositional information. Since bitumen is a challenging composition that is difficult to characterize, meaningful inputs had to be identified. In the information provided by South Bow, there was a fractional composition based on boiling point and physical properties.

To create a working model in the OLI Studio software, we must create an oil composition. To do this, we used "pseudo components" in place of much of the actual compositional information. The software allows for the input of "pseudo components" based on known key physical properties. In our case, pseudo components will possess the boiling points and fractional percent composition. The software then assigns typical hydrocarbon properties to the remaining key characteristics, including solubility in water, compressibility, and polarity. The following inputs were used:

- For the Sulfur, 5% elemental sulfur was input. We also ran the modeling experiment with an added thiol, but this did not induce any reactivity; therefore, we focused solely on elemental sulfur.
- Water concentration was input as 0.2%. This was sufficient water to exceed the solubility limit under the pipeline's conditions. You will notice that at the higher temperatures, the amount of H_2S produced decreases. This is due to the increased solubility of the water in the diluted bitumen phase.
- To simulate the naphthenic acid, a molar equivalent of neodecanoic acid was added according to the KOH used in the TAN calculation. This molecule has a pKa of approximately 5.6, which is a good analogue to naphthenic acid.
- From there, the composition was reconciled, and a survey was run across the temperature range of 75-160°F. The results are shown in the Figure 63.

Table 16: Dilbit composition based on various boiling points

Component	Normalized
Inflows	**Subtotal: 23.4469**
H2O	0.200401
C2H6	0.200401
C3H8	0.300601
i-C4H10	1.00200
C6H14	2.00401
C7H16	3.00601
i-C8H18	2.50501
H2S	0.0
C10H20O2	9.21844

Component	Normalized
Inflows	**Subtotal: 23.4469**
S8	5.01002
Pseudocomponents	**Subtotal: 76.5531**
HEAVYNAPTHA	7.01403
KEROSENEEEE	7.41483
DIESELFLUID	12.0240
BITUMENTRES	50.1002

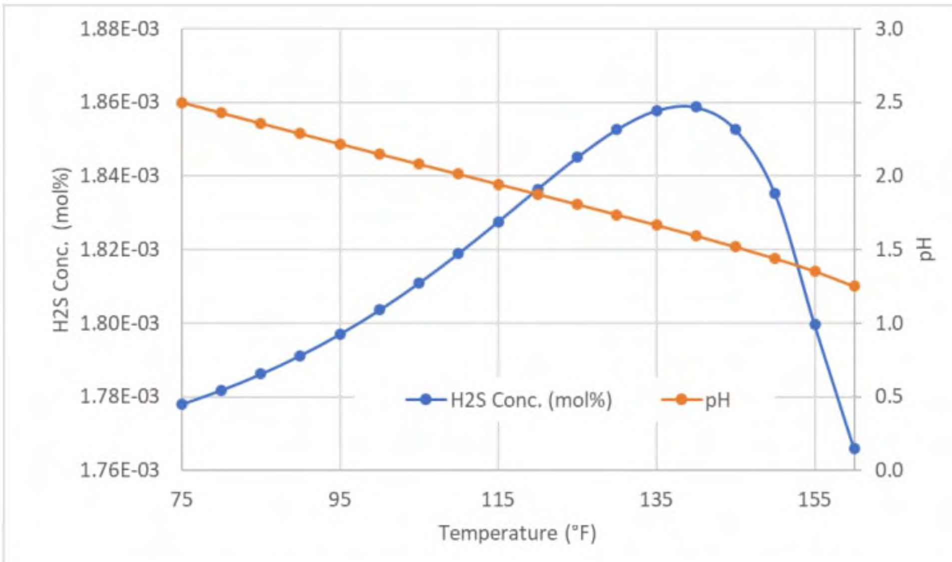

Figure 63: Plot of possible H_2S concentration in the oil phase of diluted bitumen

The conditions screened were 1,440 psig pressure and 75-160°F. The results are summarized in Figure 63. The amount of H_2S is predicted to reach a maximum around 130°F. The trend line is that more H_2S is produced as the temperature increases to approximately 135°F. It is primarily a temperature-dependent response. Above 135°F, the solubility of the water increases and combines with the oil phase. At this point, there is little or no free aqueous phase available to react with sulfur, and it is thus no longer available for reaction to make H_2S.

7.1.3 Summary

(b)(4)

[redacted]

7.2 Fracture Surface Scale Analysis

Energy-dispersive spectroscopy (EDS), Raman spectroscopy, and X-ray photoelectron spectroscopy (XPS) analytical techniques were applied to identify elements and compounds present on the ID of the pipe and on the fracture surface using the fractographic sample discussed in Section 4.2 of this report. The purpose was to understand the environment and identify clues on the fracture surface to support SEM fractographic interpretations. Spectroscopy was performed at various stages of cleaning, beginning with the as-received sample and continuing until a very light residue remained in intimate contact with the fracture surface.

7.2.1 EDS Spectroscopy

EDS was used to determine the elements present on the ID and fracture surface near the location of the greatest crack depth. Figure 64(a) shows the ID side of the fractographic sample as-received. Figure 64(b) is a higher magnification where sulfur from an EDS mapping is superimposed. Sulfur was not elevated in the pits, but rather distributed ubiquitously over all surfaces. Figure 64(b) also reflects petroleum and bitumen on the surface, obscuring the underlying mill scale.

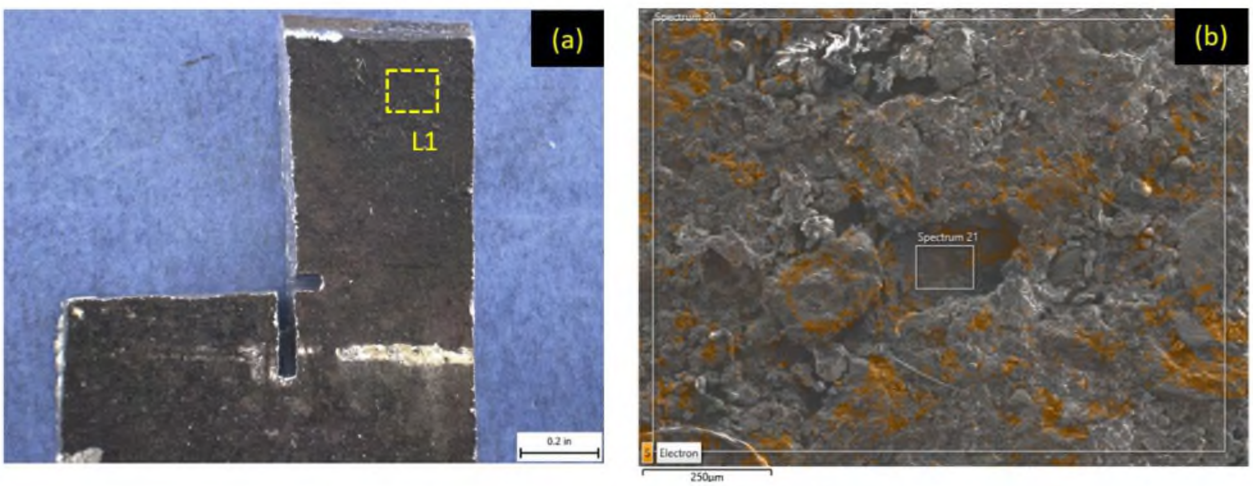

Figure 64: Spectroscopy Locations on ID, As-received

Figure 65 shows the fracture surface on the base metal side close to the point of deepest subcritical crack depth. This surface is shown in its as-received condition. As received EDS elemental composition in wt% of the ID and fracture surface is shown in Table. It should be noted that sulfur was present at an order of magnitude greater on the ID than on the fracture surface.

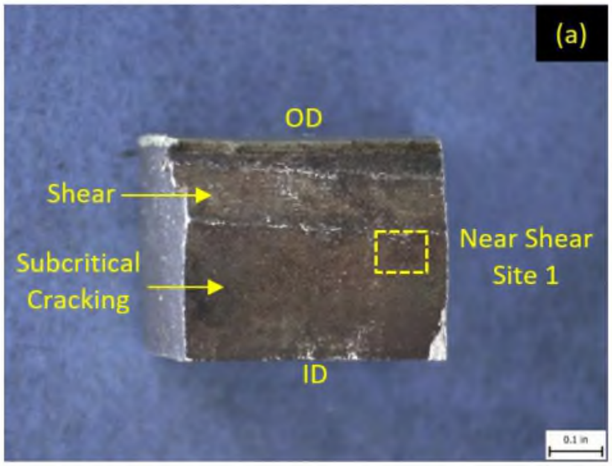

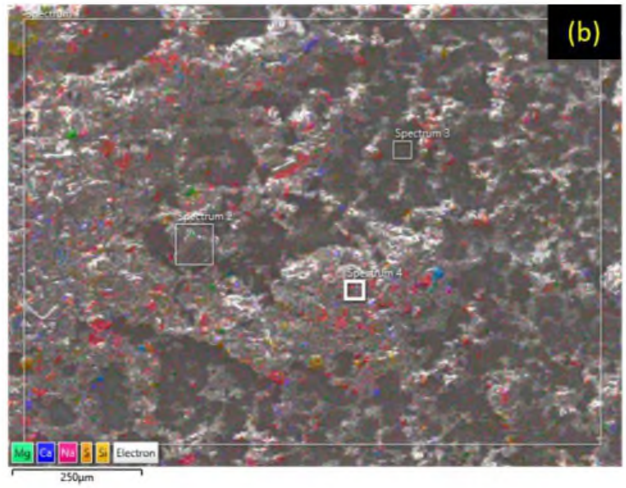

Figure 65: Spectroscopy locations on fracture face, as-received

Table 17: EDS results, as-received, wt%

	ID Surface		Fracture Surface			
Element	**Spectrum 20**	**Spectrum 21**	**Spectrum 1**	**Spectrum 2**	**Spectrum 3**	**Spectrum 4**
C	49.68	40.26	45.67	55.24	37.09	50.56
O	27.18	33.79	27.48	7.17	22.65	33.45
Na	0.72	0.31	0.82	0.46	-	1.56
Mg	0.13	-	0.19	0.18	-	-
Al	0.57	-	0.46	0.45	0.13	0.61
Si	4.22	0.25	2.29	0.7	0.29	4.17
S	8.23	5.12	0.89	0.73	0.89	0.54
CL	0.39	-	0.3	0.23	0.33	0.16
K	0.21	-	0.09	0.1	-	-
Ca	0.66	0.13	0.81	0.38	0.16	1.12
Ti	0.25	-	0.23	0.13	-	0.13
Mn	0.26	0.22	0.4	-	0.77	-
Fe	14.24	19.92	20.39	5.05	37.68	7.69
Total	100	100	100	100	100	100

7.2.2 Raman Spectroscopy

Raman spectroscopy was performed on the sample under the condition shown in Figure 65 using a ThermoScientific DX1 microscope with a 532nm laser at 1 to 3 laser power. Spectral analyses were performed with the Wiley KnowItAll tool. Several points in the region of L1 on the ID (see Figure) were evaluated. The two most common findings representing the most predominant compounds on the ID surface are shown in Figure and Figure. The Wiley tool returned “Ivory Black,” which consists of carbon-based or organic compounds, which is a mix of crude oil residue and surface compounds. Also indicated is "Burnt Umber," which contains Fe_2O_3, Fe_3O_4, and manganese oxides.

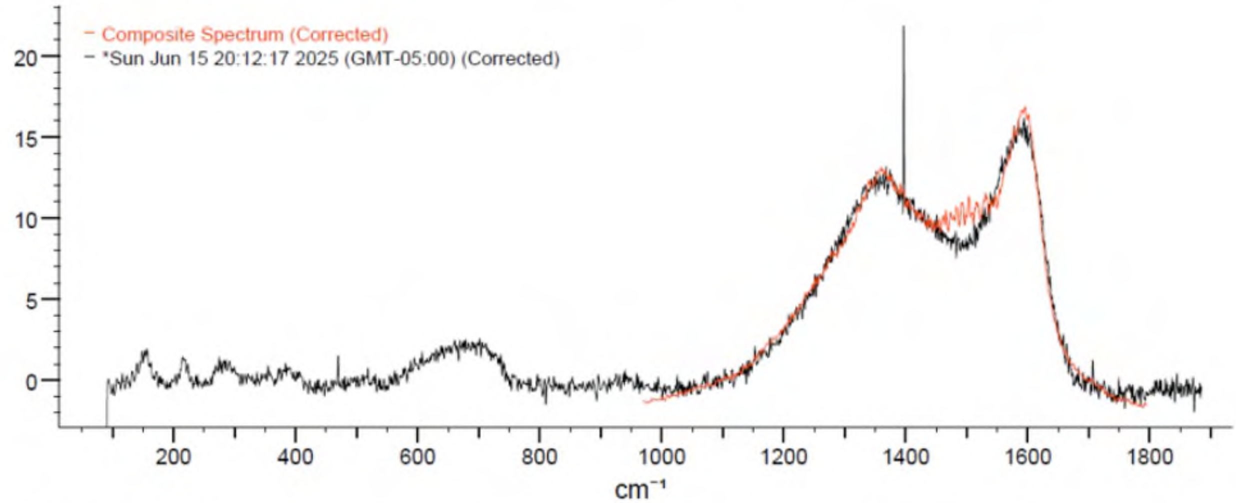

Score	Info	Ratio	Name	Chemical Structure	Spectrum
94.69		N.A.	Composite Spectrum	C	

Figure 66: Raman spectra, as-received ID surface, L1a, carbon organics

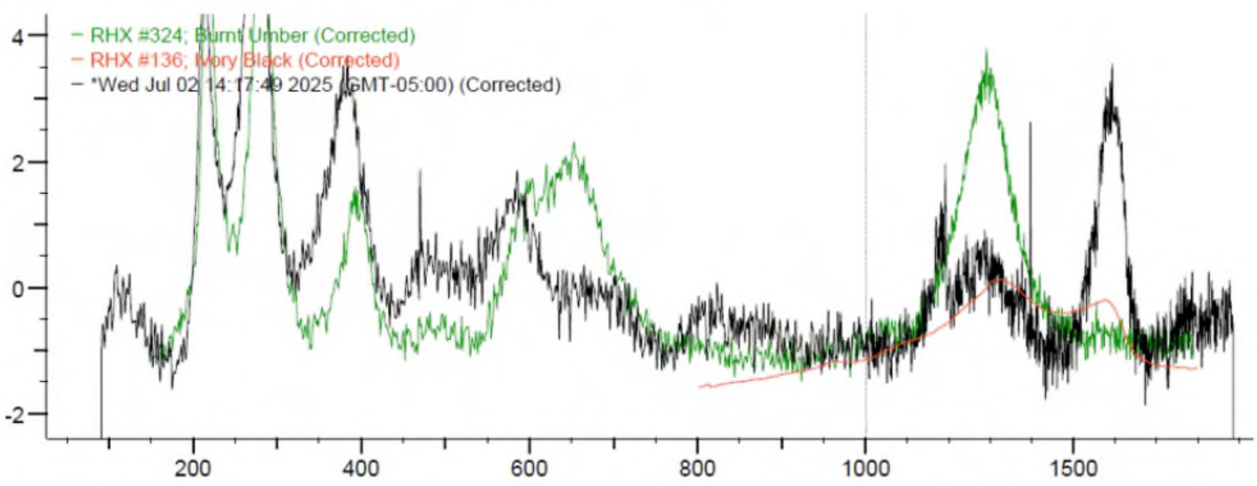

Score	Info	Ratio	Name	Chemical Structure	Spectrum
		0.55	Burnt Umber		
		0.19	Ivory Black		

Figure 67: Raman spectra, as-received ID surface, L1b, iron oxides, carbon organics, Si, Mn

The fracture returned "Mars Red," which Fe_2O_3 and Fe_3O_4, as well as silicon and a small mix of earth elements. It also includes hydrated iron oxide. Geothite, the alternative finding, is a related iron oxyhydroxide, α-FeO(OH). It is likely that Mars Red/geothite exists here as contaminants or secondary reactions and are not indicative of the failure conditions. Hydrated iron oxides may have been occluded on the surface due to the greater presence of organics.

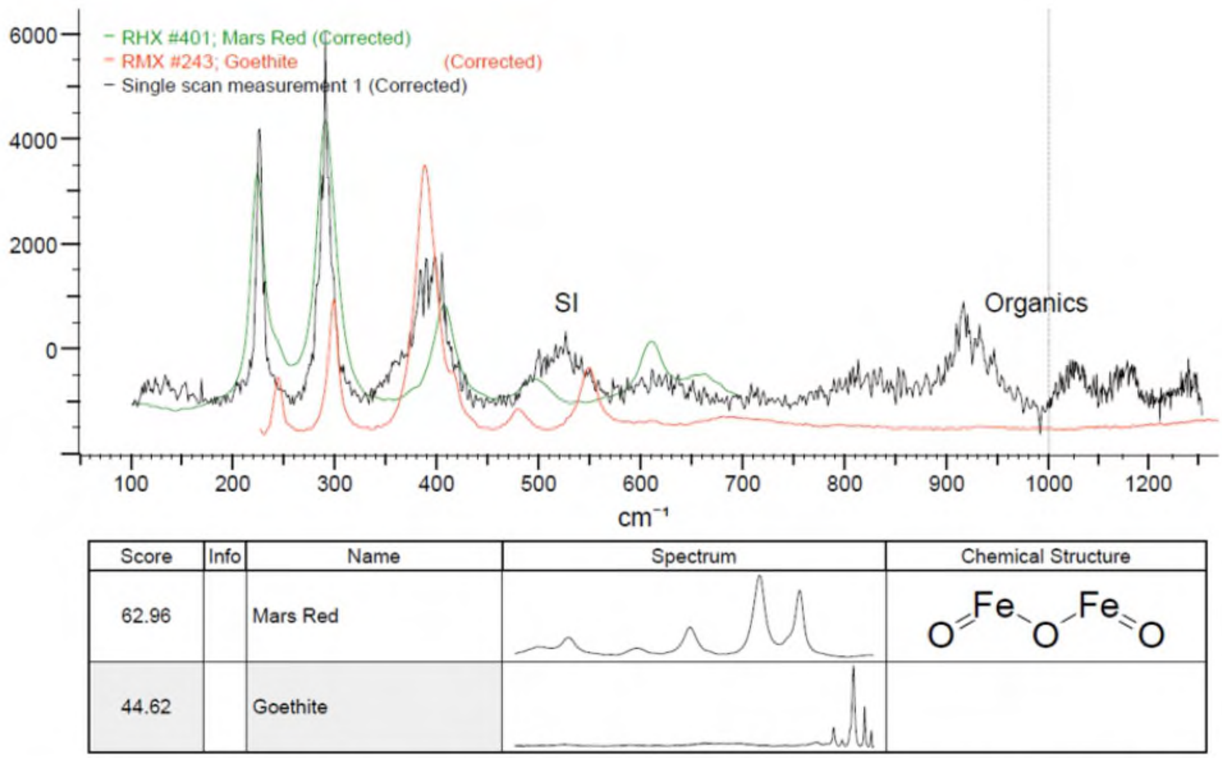

Figure 68: Raman spectra, fracture surface, iron oxides, iron hydroxide, Si, and carbon organics

7.2.3 XPS Spectroscopy

X-ray photoelectron spectroscopy (XPS) was used to identify compounds in direct intimate contact with the fracture surfaces at multiple locations near the crack tip. Due to the small excitation volume of the XPS method, the sample was sonicated in xylene to eliminate the organic compounds identified during the Raman analyses. The final surface analyzed with XPS is shown in Figure 69. A Thermo Scientific Nexsa G2 spectrometer was used to collect data, and spectra were analyzed with the Avantage software in informal (non-disclosed) consultation with the manufacturer.

EDS and Raman excite control volumes on the order of a micron, depending on the excitation applied, whereas XPS analyses excite a 10 to 15-atom layer on the surface. The larger control volumes of Raman and EDS give a greater average reading, while the XPS is highly localized in comparison. Multiple XPS survey analyses were repeated at several points along the crack tip, and chemistry and consistency were consistent between readings.

A final location near the crack tip was selected as the region of interest for in-depth analysis. An additional survey scan of the surface was collected, the location was lightly sputtered in low-energy cluster mode to remove local surface contaminants, and a second survey was taken of the freshly exposed surface. XPS survey scans are similar to EDS in that they provide quantitative elemental analysis present within the excitation control volume. Elemental quantification at the crack tip before and after light sputtering in the final region of interest, with surface contaminants removed, is shown in Table 18.

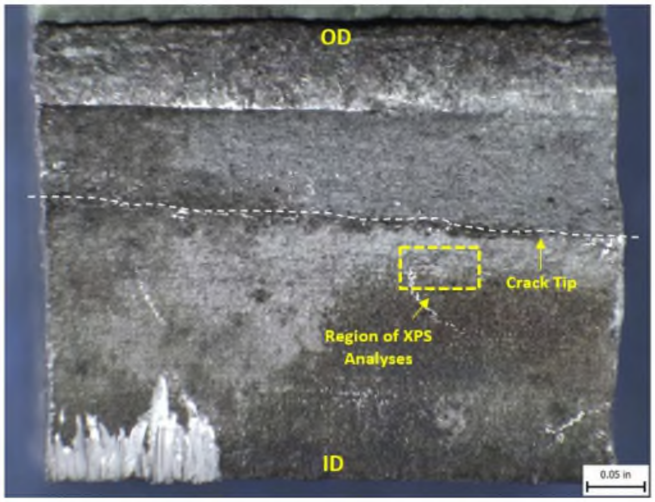

Figure 69: XPS location and surface condition

Both EDS and XPS show C, O, and Fe present in the most significant quantities. EDS and XPS suggest that Ca and S were distributed through multiple layers and present on the surface in small wt% concentrations.

The strength of the XPS method lies in its ability to measure the binding energy (BE) between chemical bonds. Deconvoluted BE peaks within a collected spectrum over the typical eV range for each element can be compared to known standards to identify exact compounds specific to an element of interest such as Fe or S. Of particular interest was the presence of iron sulfides in intimate contact with the bare metal surface, which most likely formed by the interaction of steel with H_2S in crude oil containing minute volume fractions of water.

Hydrogen evolved in the reaction to produce iron sulfides can be absorbed as atomic hydrogen into the steel, facilitating cleavage facets in susceptible microstructures. Due to the accelerated crack propagation rate, the finding of etch pits, and a significant fraction of crystallographic fracture morphology, environmentally assisted cracking is a possibility. Finding iron sulfides or iron sulfates in intimate bonded contact with the fracture surface under the contamination layer intermixed with iron oxides would be consistent with cracking in an environment containing small amounts of H_2S.

Table 18: XPS elemental survey scans results, crack tip, wt%

Survey 1, After Zylene		Survey 2, After Sputtering	
Element	**Wt%**	**Element**	**Wt%**
C1s	42.9	C1s	25.6
Ca2p	3.78	Ca2p	4.13
Fe2p	17.14	Fe2p	36.78
O1s	30.17	O1s	25.42

P2p	4.02	P2p	3.88
S2p	1.97	S2p	4.19

With XPS, determination of compounds requires the deconvolution of the spectral envelopes over the possible eV range for a given element. Deconvolution is approached per specific rules in terms of FWHM, peak ratios, spacing, etc. [33]. The NIST database was the primary source for spectral deconvolution [34].

Figure 70 shows the fitted iron or Fe2p XPS spectrum of compounds in intimate contact with the steel substrate just below the crack tip. Figure 70 is a complex mix of iron-sulfur compounds along with iron oxides. Binding energy peaks below 710 eV represent the weaker Fe2+ oxidation state [35] [36], which, in this case, are iron-sulfur reactions such as iron sulfide and iron sulfate.

The satellite peaks in Figure 70 support the identification of both Fe2+ (sulfide and sulfate) and Fe3+ (iron oxide) oxidation states [37]. The key finding by XPS is the table included with Figure 70, which shows that Fe2+ iron-sulfur reaction byproducts are present, intimately associated with the metal surface, which exist in addition to the Fe3+ iron oxides found by Raman.

A note on sputtering and the Fe2p curve: monatomic Ar sputtering at excessive energies and times can reduce oxidation states from Fe3+ to Fe2+ to Fe0 [38]. In this case, the Fe2p curve was analyzed before sputtering to establish a reference. Further, the Nexsa G2 has a lower energy "cluster sputtering" option. The combination of these precautions ensures that sputtering only removes surface contamination, and the results are unaltered.

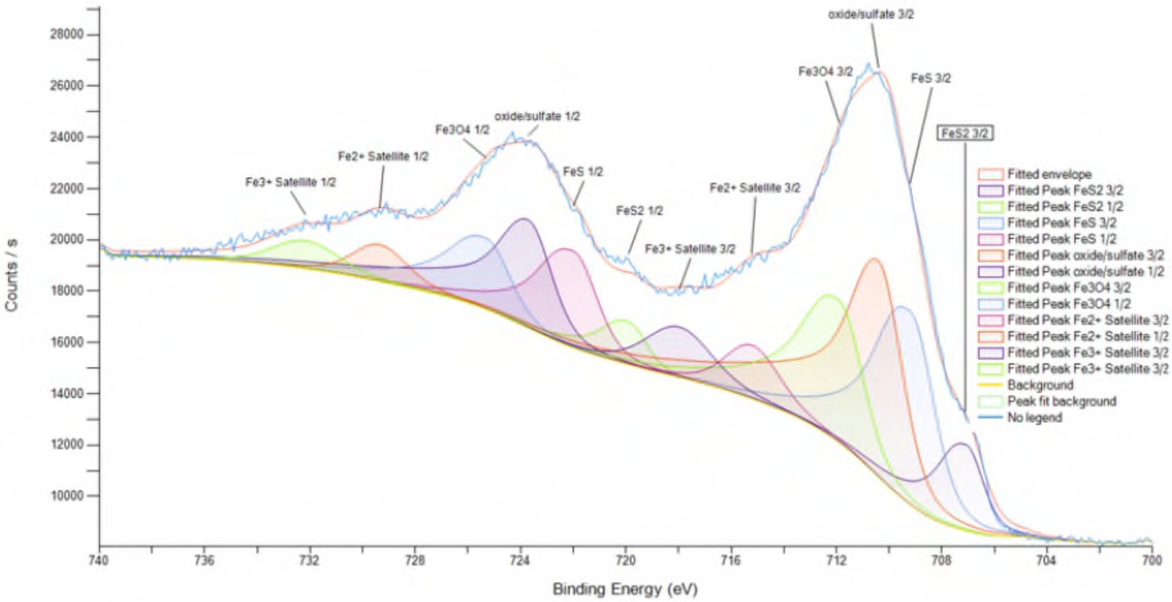

Peaks					
Name	Peak BE	FWHM eV	Area (P) CPS.eV	Weight %	Q
Fe3+ Satellite 1/2	732.17	3.00	3815.83	2.42	Yes
FeS2 1/2	719.90	2.15	4855.80	3.04	Yes
Fe2+ Satellite 3/2	715.20	2.50	6302.55	3.93	Yes
Fe3+ Satellite 3/2	717.99	3.00	7046.46	4.41	Yes
FeS2 3/2	707.10	2.15	10220.18	6.33	Yes
Fe3O4 1/2	725.31	2.99	10801.72	6.81	Yes
FeS 1/2	722.00	2.79	13088.41	8.22	Yes
oxide/sulfate 1/2	723.72	2.65	16986.62	10.69	Yes
FeS 3/2	709.20	2.79	26177.49	16.24	Yes
oxide/sulfate 3/2	710.40	2.65	34543.36	21.45	Yes
Fe2+ Satellite 1/2	729.35	2.50	4316.80	2.73	Yes
Fe3O4 3/2	711.90	2.99	22081.33	13.73	Yes

Figure 70: XPS fitted Fe2p spectra

Figure 71 shows the fitted sulfur or S2p spectra. The analysis is consistent with the conclusion derived from fitting the iron Fe2p curve. Dublets required to fit the curve correspond to the presence of iron sulfide, iron sulfate, elemental S8 sulfur, and organic sulfur mixed compounds.

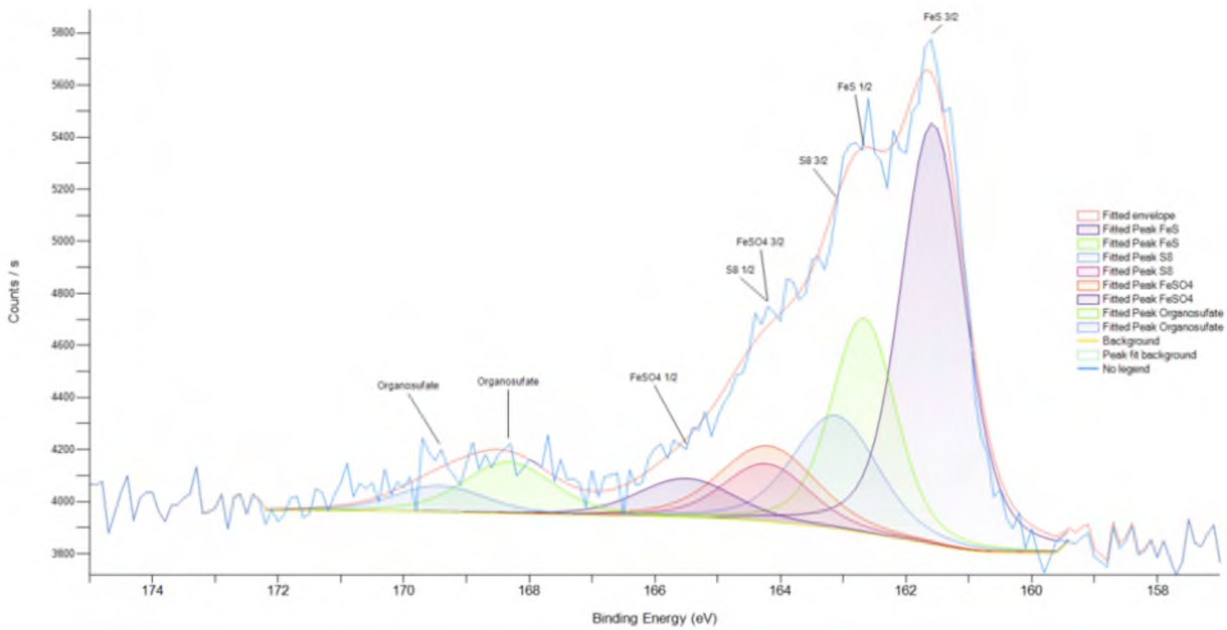

Peaks					
Name	Peak BE	FWHM eV	Area (P) CPS.eV	Weight %	Q
FeS 3/2	161.57	1.20	2277.90	37.99	Yes
FeS 1/2	162.67	1.20	1163.58	19.42	Yes
S8 1/2	164.22	1.60	415.34	6.94	Yes
FeSO4 1/2	165.50	1.80	313.54	5.24	Yes
S8 3/2	163.12	1.60	813.11	13.57	Yes
FeSO4 3/2	164.20	1.80	613.82	10.25	Yes
Organosufate	168.33	1.70	393.32	6.59	Yes
Organosufate	169.43	1.70	200.91	0.00	

Figure 71: XPS fitted S2p spectra

The C1s carbon curve was fit and reflected carbon-carbon bonds and carbon-oxygen bonds, and a small fraction of carbonates. The Ca2s was fit and showed that the carbonates existed as calcium carbonates. The O1s curve confirmed the presence of sulfates, oxides, and oxy-hydroxides previously identified in the Fe2p and S2p

Summary conclusions of the XPS analysis show that iron-sulfur reactions were likely taking place in situ at the metal substrate/environment interface in the crack preceding the failure. These findings support the possibility that an environmental or hydrogen influence may have acted to accelerate crack propagation. Iron-sulfur compounds underlie later deposits and compounds of products that later converted to iron oxides with exposure to a humid atmosphere. Sulfur in various forms, such as S8 and sulfates, was present through all layers of the compound overlying the fracture face.

7.2.4 General Conclusions of Spectroscopy

Before cleaning, the EDS, Raman, and XPS signals indicated the presence of a range of elements and compounds on the crack face. Most of these elements and compounds were considered residual crude oil products, contamination from interaction with soil during excavation, or post-failure reactions to humid air conditions and human handling.

EDS and XPS showed sulfur was ever-present in low quantities in all layers covering the crack face. EDS and Raman analysis revealed that the scale layer was contaminated with significant amounts of organics, iron oxides (and possibly iron-oxy-hydroxides), and silicon. The low levels of sulfur were likely obscured by other compounds that dominated the Raman spectra.

After Xylene sonication cleaning and removal of alcohols, bitumen, loose iron oxides, etc., the XPS spectra of residual compounds on the metal surface could be deconvoluted with confidence, confirming the presence of iron sulfide and iron sulfate bonded to the crack face.

7.3 Internal Corrosion Assessment

Blade compared the reported features and reviewed the in-line inspection (ILI) signals of three magnetic flux leakage (MFL) ILIs:

- 2012 [redacted] ILI, Axial MFL (A-MFL), the baseline inspection,
- 2016 [redacted] A-MFL, and
- 2018 [redacted] Axial + Spiral MFL (A+S-MFL)

The objective of the comparison is to determine whether any new internal corrosion features are present after those identified in the baseline inspection.

The 2012 ILI reported corrosion features consistent with internal corrosion by stagnant water left after the commissioning hydrotest, which accumulated in relatively low-elevation areas. The resulting corrosion patterns are lenticular and centered on the bottom of the pipe, with pitting occurring at the interface between the stagnant water and the air in the pipeline (before commissioning) and the transported oil (after commissioning), as illustrated in Figure 72.

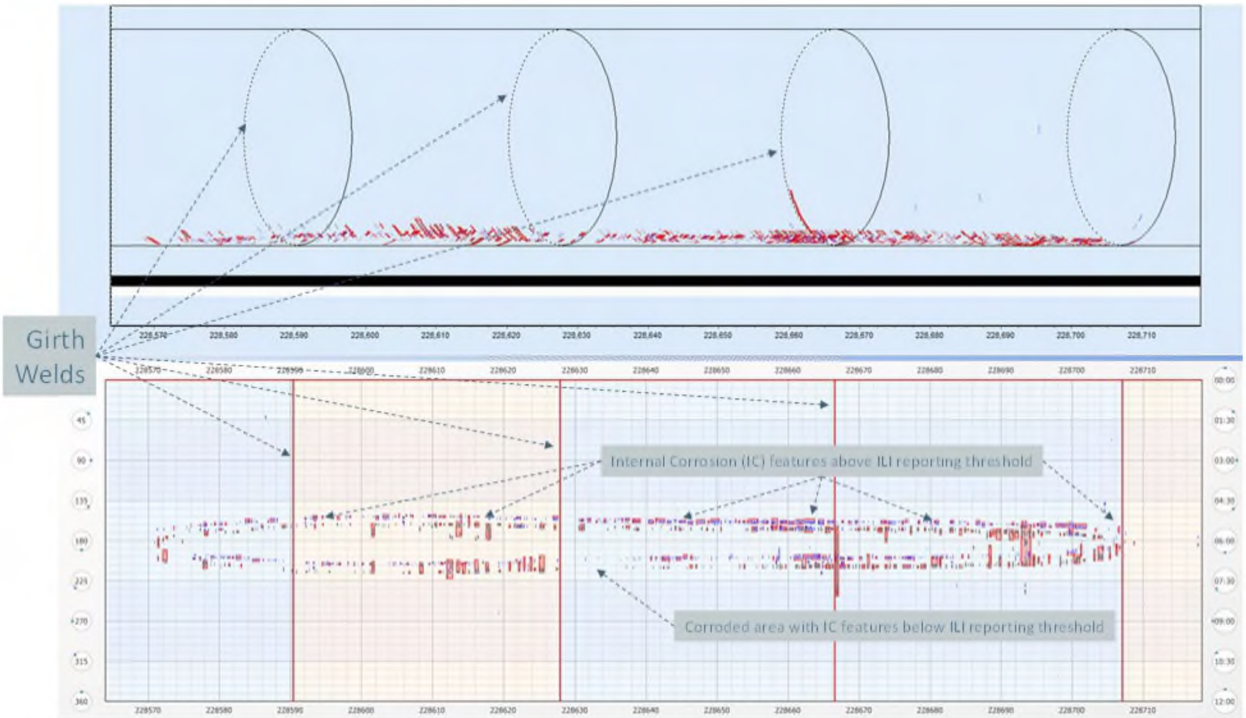

Figure 72: Lenticular internal corrosion pattern

The corrosion evaluation performed here involves aligning the ILI inspections at the girth-weld-to-girth-weld level and conducting a high-level comparison to identify areas of potential internal metal loss (IML) depth difference.

Following this assessment, a sample of features that are suspected of exhibiting growth is selected for detailed signal comparison to confirm the results of the high-level comparison. Typically, individual ML features are chosen from recent ILI data for a detailed comparison of the signal data with previous ILI data. This process is performed using the signal viewer software programs provided by each ILI vendor.

The corrosion depth comparison relies on the ILI vendor sizing, as sizing procedures and methods are unique intellectual property for each ILI vendor. However, careful signal correlation and review categorize the metal loss depth difference into three different categories:

- Evidence of new corrosion or of corrosion growth
- No evidence of growth
- Not enough information to define growth / no-growth

7.3.1 Alignment of Features and High-Level Comparisons

The purpose of the preliminary comparison is to identify new metal loss features not reported during the previous ILI, metal loss features that have significantly increased in depth, and areas of significant growth in the length or width of a metal loss feature reported in previous ILI.

To identify areas of potential corrosion growth, all of the reported metal loss features (including corrosion, manufacturing, and other ML) were subject to a first pass screening. The assessment is conducted using the standard pipeline listings provided by the ILI vendors for the current and previous ILI surveys.

Figure 2 show the overview of the aligned features with the distribution reported by both in-line inspections for the same area shown in Figure 1. In the graph, the x-axis represents the standardized absolute distance. At the same time, the stacked y-axes show the elevation of the line, the reported nominal wall thickness, and the distribution of the external and internal features in terms of the depths and orientation reported by each ILI.

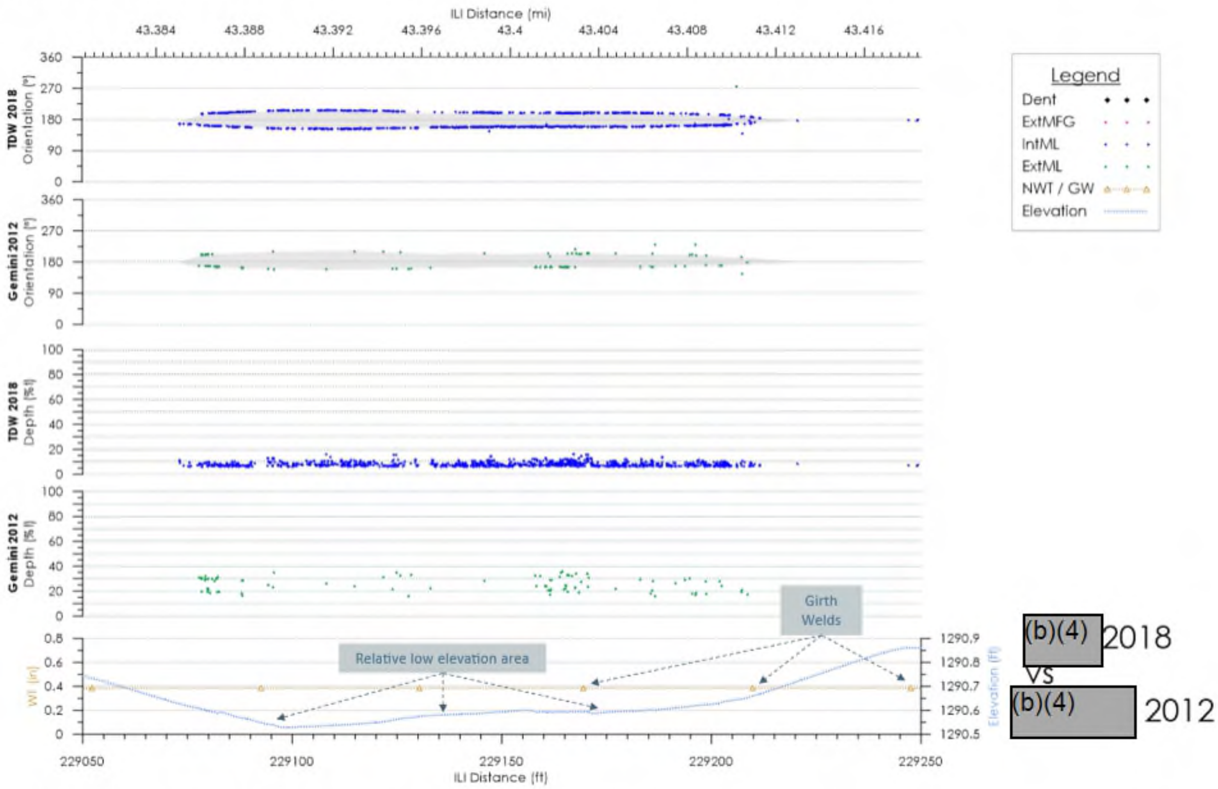

Figure 73: Example of aligned ILI features (b)(4) 2018 vs (b)(4) 2012) – Same area as Figure 72

It should be noted that the 2012 ILI listed those corrosion features as external. However, following excavation analysis, the external corrosion features were confirmed to be internal and further verified through subsequent ILIs. The differences in the number of corrosion features reported are due to varying detection capabilities and threshold settings among ILI vendors.

Finally, the number of features per joint is calculated, and the deepest feature depths are compared between ILI to identify areas of potential new corrosion or corrosion growth along the pipeline section, as illustrated in Figure 74.

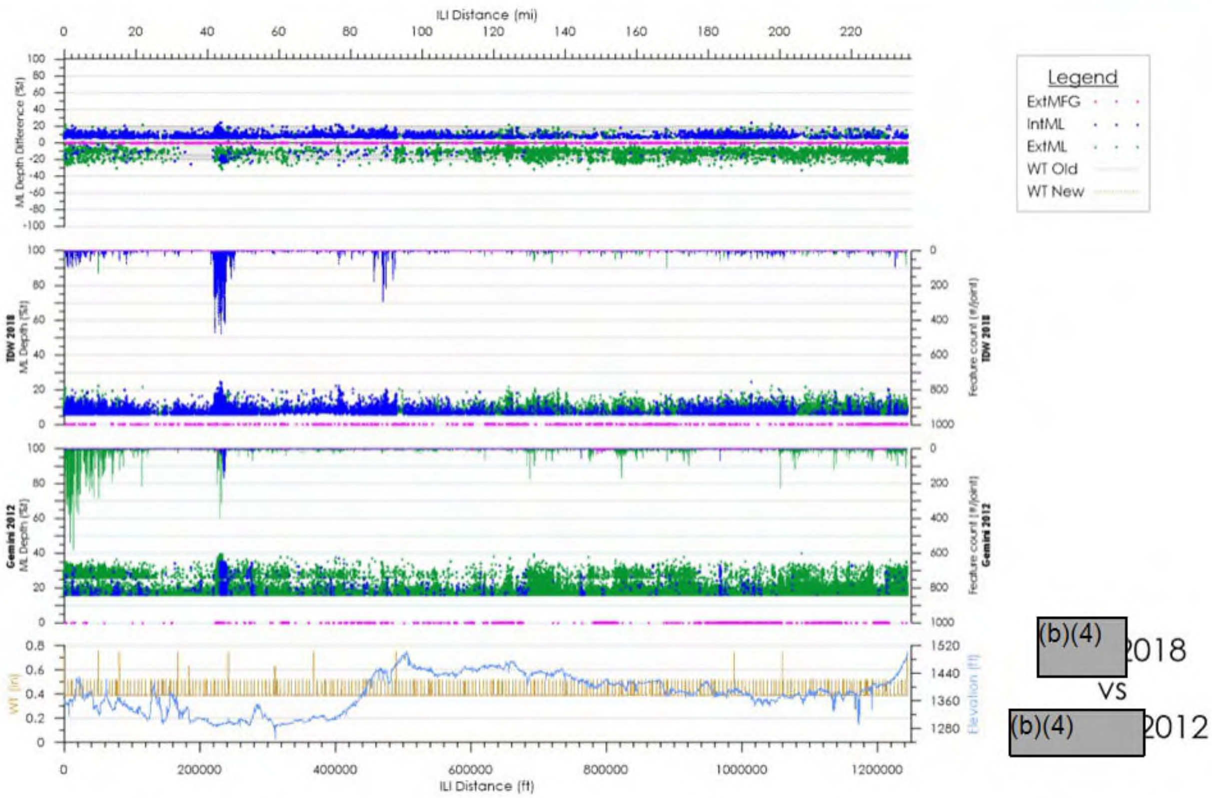

Figure 74: Depth comparison of the deepest feature per joint – 2018 vs 2012

7.3.2 Corrosion Growth/No Growth Criterion

The corrosion growth rate can be estimated by aligning and comparing ML features from two consecutive ILIs. However, any depth change cannot be considered a real corrosion growth without first ruling out that it is not due to minor differences in feature detection and sizing between the two inspection systems. In other words, the depth error tolerance for each ILI system must be taken into account to identify and quantify corrosion growth.

In theory, and assuming the depth error tolerance of each ILI system is 10% wt, the combined error tolerance is 14.1%. Based on this, corrosion growth can be assumed if the depth difference is > 14.1%. However, previous run comparison experiences indicate that corrosion growth can be assumed when the depth difference exceeds 20%. A combination of both criteria was used in this evaluation.

Figure 74 shows that most of the depth differences between [redacted]2018 and [redacted] 2012 fall within the propagated depth error of the two ILI systems (+/- 14.4%wt to +/- 20%wt), suggesting that generalized corrosion growth is unlikely.

The same comparison and signal review exercise was performed between the [redacted]018 and [redacted]016 ILIs and between [redacted] 2016 and [redacted]012, with similar results, as shown in Figure 75 and Figure 76, respectively.

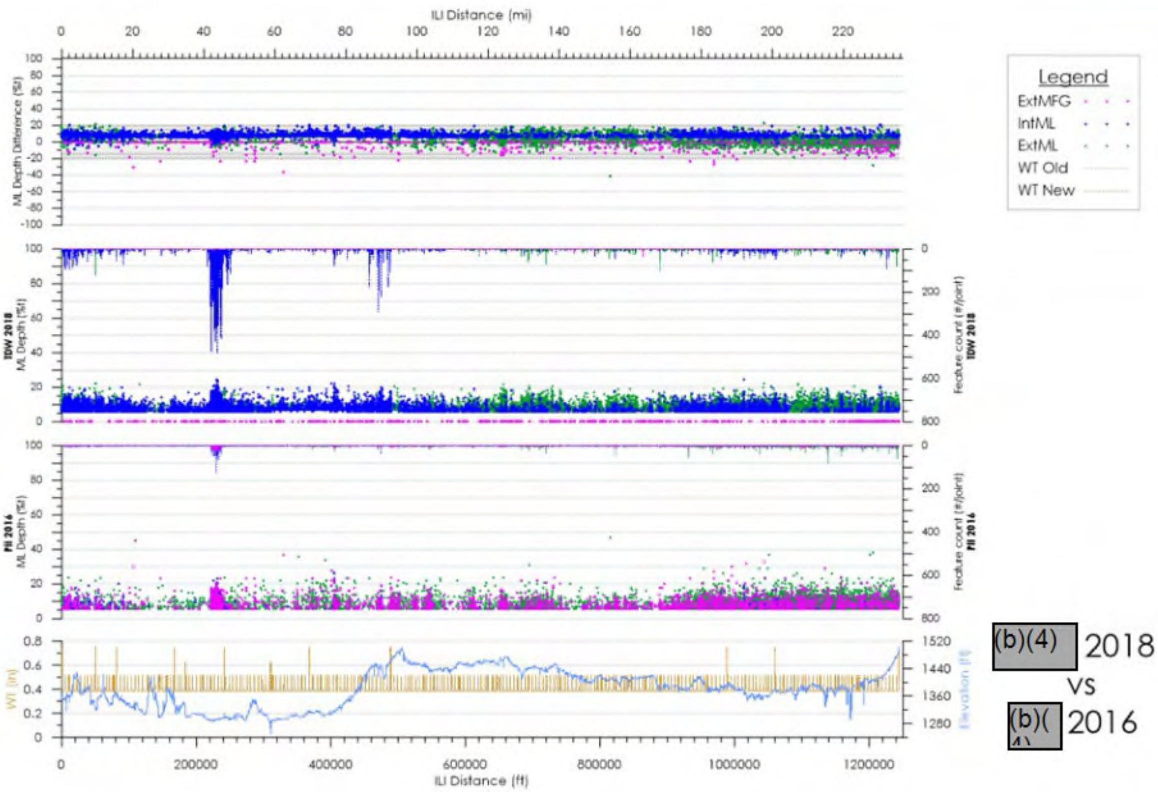

Figure 75: Depth comparison of the deepest feature per joint – 2018 vs 2016

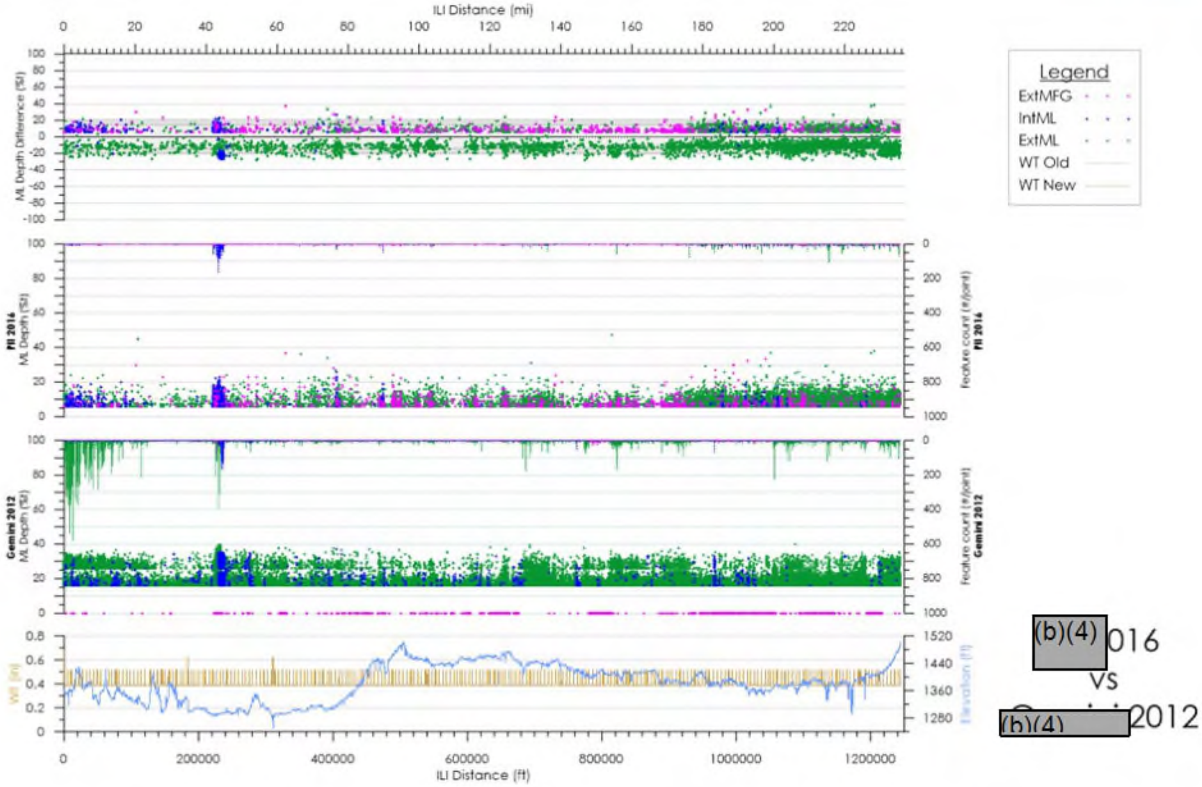

Figure 76: Depth comparison of the deepest feature per joint – 2016 vs 2012

7.3.3 Selecting Locations for Detailed Comparison

To confirm the results of the preliminary comparisons, Blade selected individual features for detailed visual comparison of the signals. This process was performed using the signal viewer software provided by each ILI vendor.

Figure 77 shows the ILI signals for the area shown in Figure 72. The blue ovals are the corrosion features (pits/boxes) that exceed the sizing and reporting thresholds and are therefore included in the ILI tallies/listings. The figure also shows areas where the signals indicate low-level corrosion that is not included in the tallies, as it falls below the sizing or reporting thresholds.

The signals along spools that contain the features previously identified in the high-level comparison are compared in detail, and the difference in signal, size, characteristics, and identification was reviewed to identify possible individual local corrosion growth.

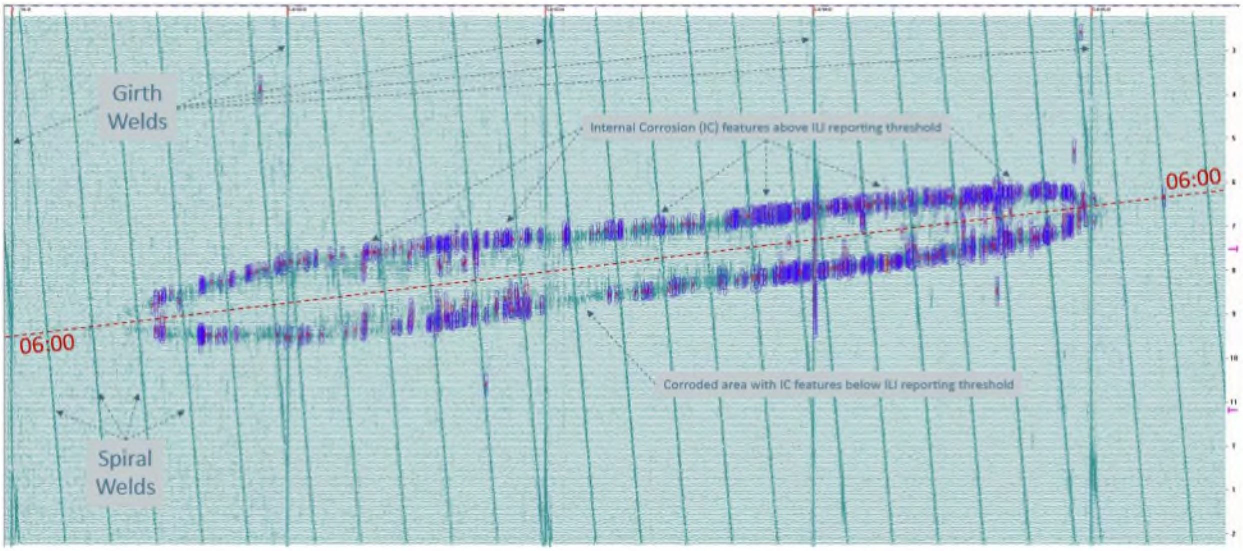

Figure 77: ILI signals for the same are in Figure 72

7.3.4 Review of MFL Signals Around GW610

Blade compared the ILI signals of the three MFL ILIs, looking for signal differences that may suggest new internal corrosion below the ILI reporting thresholds. Five joints downstream and upstream from the rupture location (GW 610 – 4 ft) were reviewed in detail. No evidence of new internal corrosion was found in them. An example of these signal comparisons (at one-joint scale) is shown in Figure 78.

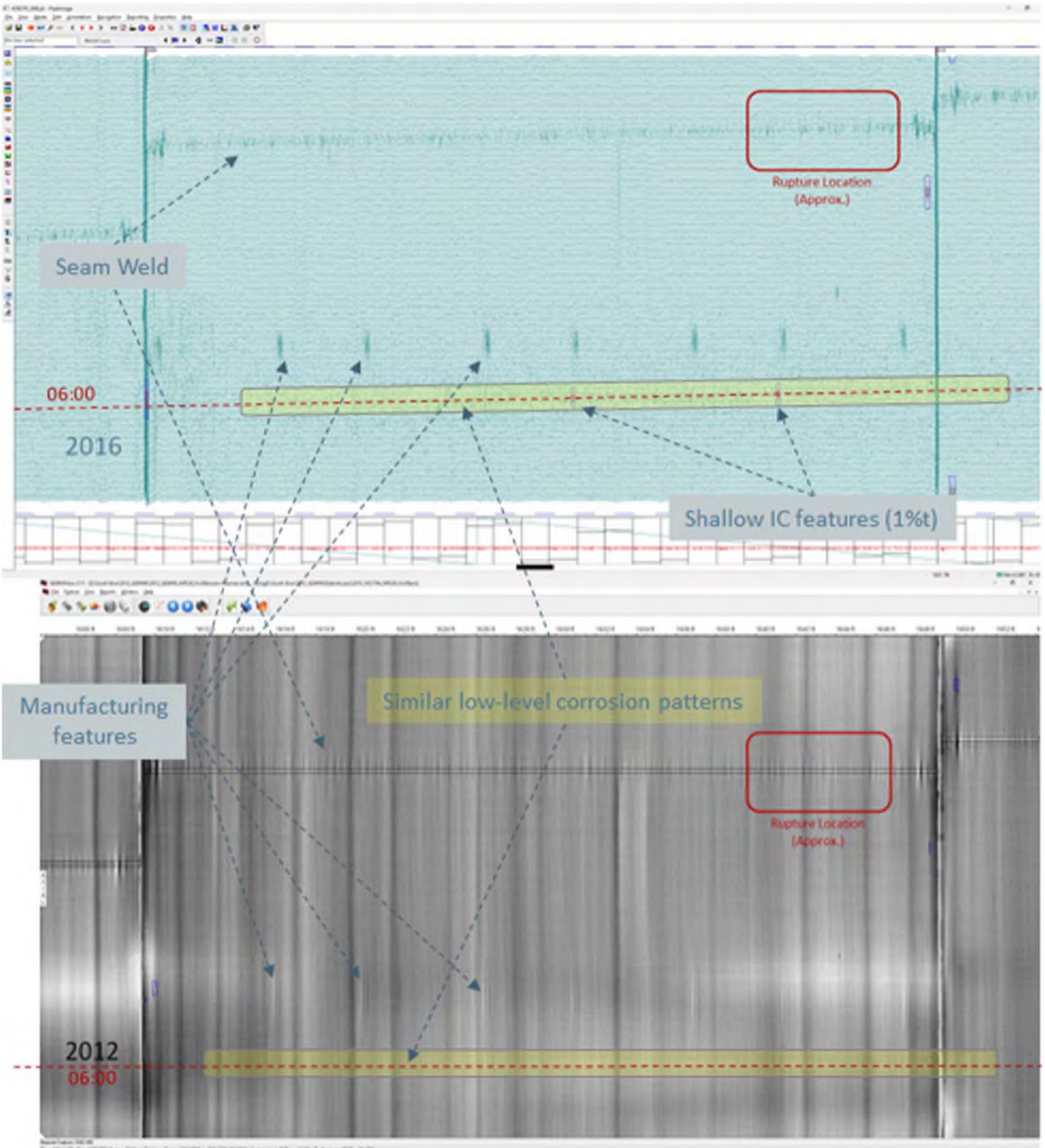

Figure 78: Example of MFL signal comparison – ruptured joint

7.3.5 Results

The ILI signals were reviewed in more than 60 joints in the first 300,000 ft (57 mi, 25% of the pipeline affected pipe segment), and no evidence of new internal corrosion was found. In other words, the internal corrosion growth and creation of new corrosion features are below the detection and sizing capabilities of the MFL ILI systems used. In consequence, the observed difference in the number and peak depth of the metal loss features reported is mainly related to:

- The different reporting thresholds
- The different identification/characterization criteria (ML vs MFG vs other vs weld anomalies, and internal vs external)
- The different sizing algorithms

A detailed review of MFL signals around GW610 didn't reveal additional internal corrosion.

7.4 Microbiological Assessment

South Bow had a leak detection tool (LDT) run on KS7, and using that opportunity, collected sludge and solids for microbiological investigation. The intent was to assess the possibility of microbiologically induced corrosion mechanisms, if applicable.

First, microbes were detected in the material, albeit at a low concentration of approximately 10^5 cells per gram. The profile of the population, which consisted of over 98% strict anaerobes, strongly suggests it is not from contaminating sources, such as surface waters or dirt introduced during collection, as both of which would have a mixed profile, including facultative anaerobes and aerobes, and not such a high percentage of strict anaerobes. Furthermore, the most abundant organisms in the sample were acetogens and sulfidogens. Acetogens are notable for their ability to fix carbon dioxide and hydrogen gas into acetate, sometimes in the form of acetic acid. The presence of acetogens indicates the sample originated from an environment with high H_2, high CO_2, but negligible O_2. Sulfidogens generate hydrogen sulfide (H_2S) under anaerobic conditions. H_2S is a known corrosion-associated chemical. Taken together, a population including sulfidogens and acetogens would be expected to have some capacity for MIC (microbially influenced corrosion). The table below is extracted from the detailed Ecolyse report.

(b)(4)

[redacted]

Figure 79: Image of the table of the type of microbes in the Metagnomics assessment

However, before this conclusion can be drawn about the KS7 LDT pipe solid sample, it is essential to note that while organisms were present in the sample, they were not demonstrated to be metabolically active, based on culture analysis by the most probable number (MPN) method. It is possible that the negative growth results were a product of these highly specialized organisms being too fastidious to grow under the basic standard conditions. Typically, MPN is set up by eluting the sample in buffer and injecting it into culture vials. The process is not conducted under strict anaerobic conditions, but rather is routinely set up on the bench, which allows for some oxygen ingress into the culture vial. With a more typical sample, the facultative anaerobes also present in the sample quickly consume any oxygen introduced during sample collection and processing, thereby generating the anaerobic environment that allows for the growth of strict anaerobes. However, facultative anaerobes were not identified in the sample, and thus, no route for oxygen scavenging was present.

In addition to the organisms not growing in culture, another line of evidence that raises questions about the metabolic activity of the microorganisms in the sample is the nature of the material itself. The oils transported in this particular pipe are known to have an extremely low water content, and water is required for the organisms to be metabolically active.

If so, the bacteria identified in the sample could have been present in the upstream oil separation process, but are not currently active during transport through the pipe.

Therefore, while the population of organisms in the sample is consistent with that of a population that causes MIC-associated issues, the lack of support for metabolic activity in the pipe itself means there is insufficient evidence to clearly state a role of the bacteria in any ongoing corrosion events within the pipe.

7.5 Summary Conclusions

These are some key conclusions from the crude oil environment assessment.

1. (b)(4) [redacted]
2. [redacted]
3. A detailed assessment of multiple magnetic tool runs indicates that the internal metal loss has remained the same as it was following hydrostatic testing. If there is any additional internal corrosion, it was below the threshold and the tolerance of the MFL technologies.
4. Microbiological assessment of the sludge from KS7 revealed microbes that can cause MIC; however, they don't appear to be metabolically active. The small quantity of water and the MPN results show that these microbes may not be active.

8 Manufacturing and Transportation

8.1 BERG Steel Pipe Facilities and Context

Berg Steel Pipe Corp., located in Panama City, Florida, manufactures longitudinally welded, large-diameter pipe with diameters ranging from 24 in. to 64 in. and wall thicknesses from 0.312 in. to 1.500 in. Double-jointing to 80 ft lengths was performed by Midwestern Pipeline Services, and external coating by EB Pipe Coating, all on the same Panama City campus.

- Pipe was supplied under Pipe Purchasing Agreement No. 5165 (TransCanada and Berg), with three production windows: V-08-32a (May 10–31, 2008), V-08-32b (Jun 1–Jul 31, 2008), V-08-32c (Aug 1–Sep 12, 2008).
- Order placed to Southbow TES-PIPE-SAW-US (Rev 0, 2006) for U.S. deliveries and TES-PIPE-SAW Rev 1/CSA Z245.1-07 for Canada, alongside API 5L, 43rd Ed.
- Keystone pipeline order covered 30 in. (762 mm) OD pipe in 0.386 in., 0.516 in., and 0.622 in. WT, Grade X70 / CSA 483 Cat II.
- The raw material plate was produced at IPSCO (Mobile, AL; electric arc furnace (EAF)) and Mittal Steel (Burns Harbor, IN; basic oxygen furnace (BOF)). Plates were thermo-mechanically rolled (TMCP) without subsequent heat treatment.
- Berg used SAWL (double-submerged-arc welded, with one longitudinal seam) and three-roll/pyramid bending, along with non-expanded pipe. The forming line includes edge milling to double-Y bevel, pyramid rolling, edge crimping, CNC tack-closure with laser seam tracking, followed by ID, then OD SAW.
- Plate heat/serial numbers, as well as a unique pipe number, are maintained in Berg's manufacturing facility computer tracking system, carried through the forming and inspection process; double-joint numbers and acceptance are also captured.

8.2 Review of Manufacturing Pipe Standards and Specifications

The manufacturing and release of Keystone DSAW line pipe were controlled by four key documents:

1. TES-PIPE-SAW-US (Rev. 0, 2006) [39], TransCanada's purchaser specification that supplements API 5L with tighter workmanship, inspection, and testing requirements.
2. BERG MPS-BSPC-TC-03 [5], the mill's manufacturing procedure specification and quality plan that implements those "shall" requirements and the inspection/test plan on the shop floor.
3. API 5L (2004, 43rd Ed.) [40], the base product standard defining pipe and weld-seam tolerances and acceptance criteria.
4. PHMSA Special Permit 2006-26617, which establishes project-specific regulatory conditions (e.g., design/operating limits and added QA/ILI/hydrotest requirements).

In practice, API 5L provides the baseline, TES-PIPE-SAW-US adds purchase-specific requirements, the MPS operationalizes them at the mill, and the PHMSA special permit imposes additional federal conditions where requirements overlap; the most stringent governs.

For Keystone's DSAW line pipe, API 5L was the base product standard. For U.S. delivery, TransCanada ordered to TES-PIPE-SAW-US [39] in combination with API 5L, 43rd Edition [40]. For Canadian delivery, they ordered to TES-PIPE-SAW (Rev.1) with CSA Z245.1. Berg's Manufacturing Procedure Specification (MPS-BSPC-TC-03) was explicitly written to "reflect the most stringent requirements" across those purchaser specifications and standards, and in accordance with a certified quality system (ISO 9001, API Q1). The MPS specifies continuous-cast, TMCP raw material plate and non-expanded, double-submerged-arc longitudinal welding (DSAWL).

The pipe purchase agreement (PPA) [41] between TransCanada and Berg formalized the standards stack above and required conformance to TES-PIPE-SAW-US, API 5L (43rd), and the PHMSA Special Permit conditions. Project records show that PPA #5165/5590 was executed in 2007 for X70 PSL2 SAWL pipe. Production proceeded following pre-production meetings and approval of Berg's MPS.

As documented in Table 1 of "Manufacturing Procedure Specification Documentation / NDE Procedure Documentation," PPA #5165/5590 (Berg Steel Pipe Corp., Panama City, FL), TransCanada reviewed and approved Berg's NDE procedures for the Keystone order in accordance with the terms of TES-PIPE-SAW Rev 1 (Clauses 5.4.9, 12.1.5, 12.5.7) and TES-PIPE-SAW-US Rev 0 (Clauses 5.7, 9.8.3.4, 12.4).

The program included automatic ultrasonic testing of the seam with manual shear-wave UT confirmation scans as required (QC-NDE-003; QC-NDE-004), radiography including film and digital imaging for end zones and targeted locations (QC-NDE-005, QC-NDE-016, QC-NDE-018), magnetic particle inspection with calibrated yokes for surface indications (QC-NDE-007; QC-NDE-010), and lamination testing at ends and along the body using UT, with a defined 6 dB drop sizing method (QC-NDE-008; QC-NDE-008 Appendix A; QC-NDE-012). Pipe-body UT coverage and shear-wave end testing of circumferential areas were also included (QC-NDE-009; QC-NDE-013).

Visual/dimensional checks were documented at the final inspection (QC-NDE-006), and each joint underwent hydrostatic testing in accordance with the mill procedure (OP-PROD-014). These activities were implemented in accordance with the approved Manufacturing Procedure Specification and Quality Plan (MPS-BSPC-TC-03).

8.3 DSAW X70 Pipe Manufacturing Process

One of the key steps in the manufacturing process is crimping, during which the edge curvature and local roundness are established. Suppose the resultant curvature/roundness at the longitudinal edges of the open pipe deviates from that of the target pipe diameter. In that case, workmanship imperfections, such as offset plate edges, out-of-line weld beads, and angular misalignment, can arise downstream in the manufacturing process.

During crimping, as shown in Figure 80, several seam-geometry risks can be introduced in one step. If the edge curvature is mismatched, the seam can "peak" (roof-topping), so the edges meet as a ridge that concentrates strain at the weld toe and can initiate toe cracking.

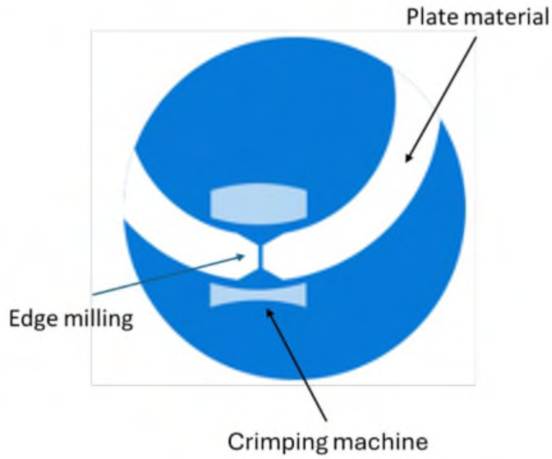

Figure 80: Edge crimping

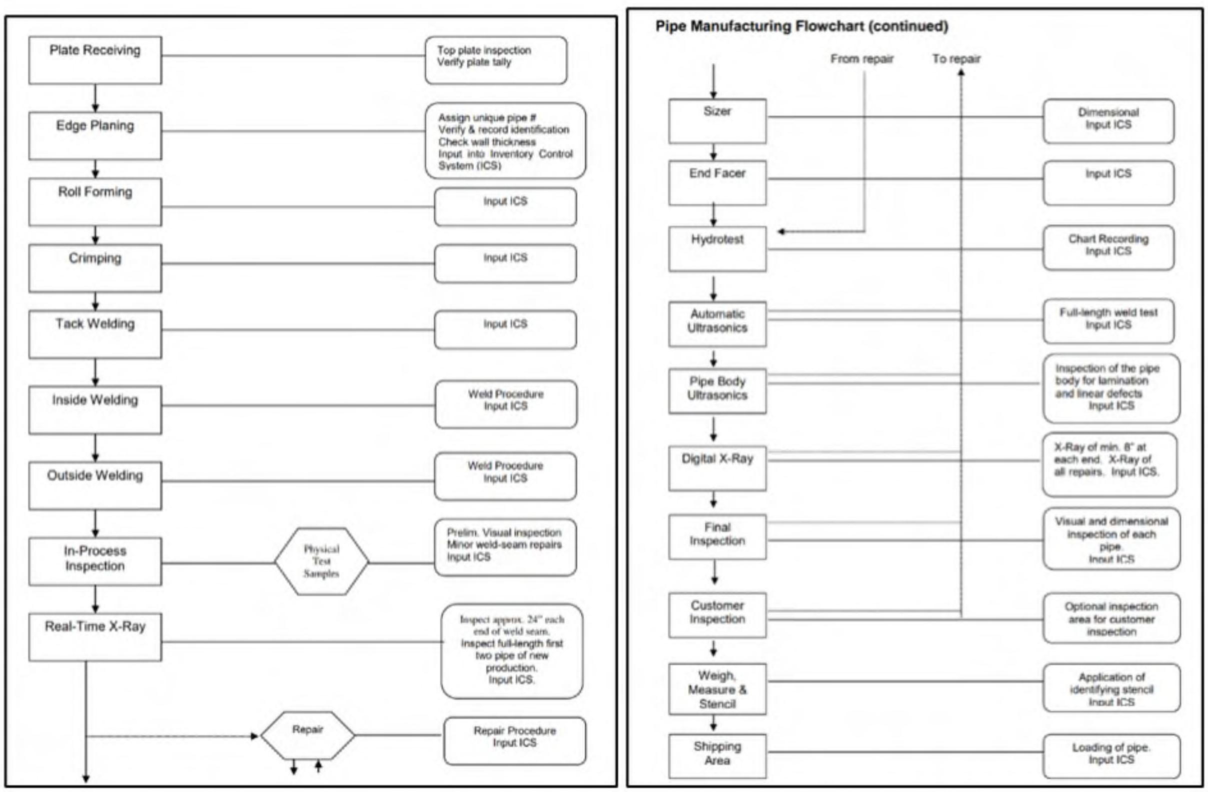

Figure 81 Manufacturing process flow chart (MPS-BSPC-TC-03 Rev 1) [5]

Camber, twist, or waviness can create radial offset (hi-lo) between the edges, adding bending stress in pressure service and a strong fatigue driver under cycling. Excessive crimper load or worn tooling can cause local thinning or work-hardening at the edge, degrading fit-up and toughness. Poor edge forming may also leave ovality near the seam. Finally, over-crimping can distort the weld and DSAW fusion quality. Mills manages this crimping operation by appropriate tooling selection, tight dimensional limits (offset/peaking/ovality), seam-tracking at weld, and NDE, all captured in Berg's MPS-BSPC-TC-03, Rev. 1. [5].

8.4 Workmanship and Defects

The Keystone line pipe was manufactured using double-submerged-arc welding (DSAW): an automatic tack weld to close and align the can, followed by an inside SAW pass and a subsequent outside SAW pass. All welding was performed in accordance with written, qualified procedures (ASME Section IX, supplemented with additional toughness and hardness qualifications). Consumables were lot-controlled and traceable: the seams used 1/8-in solid wires, such as Lincoln L61 or L70, with Lincoln 761 bonded flux. The wire/flux was stored in a conditioned room, issued from sealed bags, and moisture-checked. Additionally, no re-crushed flux was used. The inside pass was deposited using a stationary multi-arc head while the pipe was transported on rolls. A guide wheel and automatic stick-out control maintained the torch position, and instruments were calibrated on a regular schedule. However, welding is a controlled but variable process; no weld seam is guaranteed 100% defect-free, so it's essential to understand the types of weld discontinuities and the acceptance limits that govern release. For SAWL seams, the critical dimensional and metallurgical items include radial offset (high-low), bead misalignment, reinforcement/undercut, internal taper, peaking/flat spots, and fusion-related defects (lack of fusion/penetration, porosity), as well as surface issues such as arc burns. Acceptance should follow the most stringent of the API 5L, the purchaser's specification (TES-PIPE-SAW-US), and the mill's MPS.

(b)(4) [redacted]

8.4.1 Radial Offset (Plate Edge Offset)

When welding the longitudinal plate edges of the formed open can, a radial offset occurs when the centerlines of the abutting plate edges are not perfectly aligned. This misalignment is also known as "hi-lo". As per recent API 5L standards, radial offset (hi–lo), where the two plate edges are out of line through the wall, so one side sits higher or lower at the joint as shown in Figure 82 (a). Misalignment at the longitudinal weld seam can appear in four ways as shown in Figure 82 (b). These schematic pictures are extracted from API5L 44th editions because no figures are provided to the manufacturer in the API 5L 43rd Edition. It explains the basic idea of seam setup, where two plate edges are joined, ensuring they align through the wall so that the joint doesn't leave the wall any thinner than what the specification allows.

Similarly, weld bead misalignment, where the inside and outside weld beads are not centered on the same line and are therefore non-colinear, and angular misalignment (often called peaking or roof-topping), where the pipe surface near the seam departs from a smooth cylindrical contour and forms a ridge or peak along the weld.

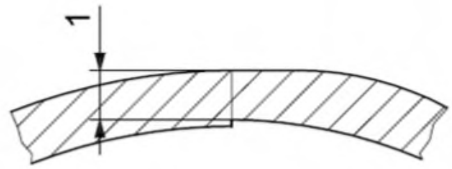

Key

1 remaining wall thickness at the weld

a) Radial offset of strip/plate edges of EW and LW pipes

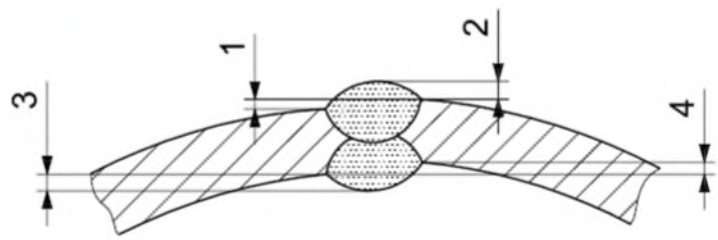

Key

1 outside radial offset

2 height of outside weld bead

3 height of inside weld bead

4 inside radial offset

b) Radial offset of strip/plate edges and height of weld beads of SAW pipe

Figure 82: Radial offset as per API 5L [API 5L 2007] [42]

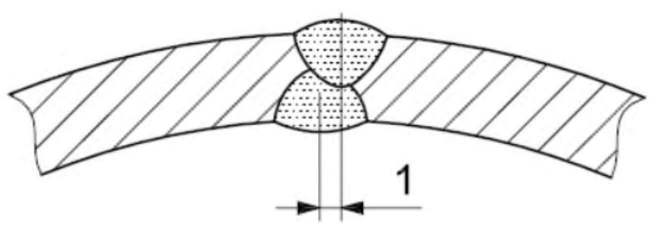

Figure 83: Misalignment of SAW welds [API 5L 2007] [42]

One of the key findings from previous Edinburg failure analysis (RSI–027–1901) was that the off-spec radial offset at the origin (b)(4) (b)(4) [redacted]

During hydrotesting, elevated local stresses can cause a first-cycle failure to occur when sharp imperfections are present. Finally, internal steps can trap deposits and create crevice conditions, while external peaks complicate coating application and concentrate coating stresses, further increasing the risk of long-term deterioration.

As per the purchase agreement PPA–5165–5590 and TC Energy specification TES-PIPE-SAW-US, the acceptance limits include radial offset (hi/lo) ≤ 10% of wt.

Over the years, from the 2004 (43rd) edition to the current API 5L 46th edition, the standard has steadily tightened and clarified manufacturing acceptance criteria as given in the Table 19.

Table 19: Comparison of radial offset limits as per standards

Standard	Limits of radial offset
API 5L (43rd, 2004)	"Offset of plate edges" = misalignment of plate edges in the weld seam. For filler-metal welds: if t ≤ 0.500 in (12.7 mm), max 1/16 in (1.6 mm); if t > 0.500 in, max min (0.125 t, 1/8 in = 3.2 mm).
API 5L (44th, 2007)	"Radial offset of strip/plate edges" shall not exceed Table 14 of this edition for SAW/COW: t ≤ 15.0 mm → 1.5 mm; 15.0 < t ≤ 25.0 mm → 0.1 t; t > 25.0 mm → 2.5 mm. (Also defines measurement geometry in Fig. 4.).
API 5L (46th, 2018)	Same Table 14 limits as 2007; text reiterates the requirement and the measurement references to Fig. 4.
TransCanada TES-PIPE-SAW-US (Rev 0, 2006)	"Offset of plate edges": max = 10% of wt at any location/all wall thicknesses (single rule).

8.4.2 Out-of-Line Weld Bead (Off Seam Weld)

As per API 5L 43rd edition [40], out-of-line weld bead (off-seam weld) shall not be the cause for rejection, provided that complete penetration and complete fusion have been achieved, as indicated by nondestructive inspection.

An off-seam weld bead by itself (i.e., lateral shift of the bead) does not increase stress at the weld toe/root provided two conditions are met: (a) the joint has complete penetration and fusion, and (b) the through-thickness alignment and contour (radial offset/hi-lo, peaking) remain within acceptance criteria. In that case, the local stress concentration is governed mainly by bead shape and any step or peak in the base metal, not by the bead's lateral position, and API allows acceptance on that basis.

The risk arises when an off-seam bead is a result of tracking/fit-up issues that produce misalignment or fusion defects, which becomes a credible crack-initiation driver.

8.4.3 Geometric Deviations

As per the TES-PIPE-SAW-US geometric deviations (7.8.15) [39] from the normal cylindrical contour of the pipe, which occurs because of the pipe forming process or manufacturing operations (e.g., flat spots, peaks) shall not exceed 1/8" (3 mm), measured as the gap between the extreme point of the deviation and the prolongation of the normal contour of the pipe.

According to the TES-PIPE-SAW-US flat spot and peaking requirement (7.2.2), the weld on the failed joint did not meet the requirements. The peaking at the failed location creates a geometric deviation that exceeds the 5/64 in. allowed by the standard at the weld near the pipe ends. Details of the peaking (angular misalignment) are discussed in Section 5.4.2.

Geometric measurements of seam welds checked using macro examination near the failure region are within specified limits for radial offset, out-of-line weld bead, and cap height per API 5L 43rd edition.

The Anderson lab reported the measurements that are in line with the API and TES specification, as shown in Table 10 and Table 11.

8.5 Changes API 5L 2004 43rd ed to API 5L 2018 46th ed

Between the 2004 [3] and 2018 [43] editions, the API 5L standard transitioned from a process-specific approach to a unified, ISO-aligned framework. It formally defines 'radial offset/misalignment' and related seam weld features. Figure 82 and Figure 83 illustrate the methodology for measuring radial offset, introduced in the 2007 edition of API 5L, which established consistent acceptance/rejection criteria that inspectors can apply uniformly across mills.

The latest API 5L editions emphasize end squareness and smooth internal transitions at the seam. The intent is to avoid sharp steps or mismatches at the weld root that can impact fusion quality, toughness, or NDE reliability.

By 2018, API 5L standard spells out clearly when repairs are allowed, how they must be qualified, who may perform them, what documentation is required, and what post-repair examinations must be done (including re-tests when needed). This reduces variability and raises confidence in the integrity of any repaired seam.

Latest editions tightened expectations for written procedures (WPS/PQR), essential-variable control, consumable handling, and purchaser visibility. That raises the baseline quality system around welding, not just the weld bead itself.

Terms like undercut, arc burns, lack of fusion/penetration, laminations breaking into the bevel, geometric deviations near the seam, etc., are defined with clearer acceptance criteria (acceptable as-is, conditional acceptance, or mandatory repair/cut-out). This reduces ambiguity on the shop floor and improves the weld quality.

In summary since 2004 43rd edition to 2018 46th editions the standard moved from process specific, based limits (2004) to ISO-aligned, figure-based measurement and prescriptive repair/verification (2007–2018). That evolution makes seam geometry checks clearer, weld repairs safer and more auditable, to achieve overall welding quality more consistent across pipe mills.

8.6 Manufacturing Surveillance

Manufacturing surveillance was maintained throughout production at Berg, daily reports were issued, and production meetings were convened to review findings and implement necessary actions. Due to special permit conditions, PHMSA representatives were allowed to visit the Berg manufacturing facility. The full details of manufacturing surveillance and production records can be found in this document, DMP ENC V-08-32 [44].

Berg's activities are governed by its manufacturing procedure specification and Quality plan (MPS-BSPC-TC-03, Rev. 1). The inspection test plan (ITP) lays out the mill flow from plate receiving and edge planing through forming, tack/inside/outside SAW welding, in-process checks, real-time X-ray near the ends, sizing, end facing, hydrotest, automatic UT of the seam, pipe-body UT, digital X-ray, final inspection, and customer inspection/ship-release steps with data capture into Berg's computer tracking system at each station.

Each pipe receives a unique serial number; the mill's CTS system records special customer requirements, inspection codes, remarks, and can place individual pipes on "hold" status with coded reasons i.e., a mechanism to track and disposition non-conformances and repairs with full traceability.

The MPS/ITP calls for hydrostatic testing with chart recording, full-length automatic UT of the longitudinal seam, pipe-body UT for laminations/linear indications, and digital X-ray followed by a final visual/dimensional inspection before release. Acceptance is tied back to API 5L/ CSA Z245.1 references in the plan.

Near the pipe ends, a real-time X-ray is used as an internal process control and to examine any local repairs; images are digitized and logged. At the end of the line, digital radiography and UT of the pipe ends (straight-beam for laminations and shear-wave for linear indications) are performed; the plan also specifies operator qualifications for UT (ASNT-TC-1A) and typical standards/calibration practices, with image-retention requirements.

A full-length internal and external visual inspection is performed, with checks on weld condition, bevel/land, straightness, and roundness. "Peaking" (roof-topping) near the seam is measured using a radius template as part of the pipe release criteria.

Any weld seam repairs must follow qualified procedures compliant with API 5L/CSA Z245.1, TES-PIPE-SAW-US, with recorded preheat/electrode control and mandatory re-examination (RT, hydrotest, and UT) of the repaired zone, plus explicit restrictions on what may be repaired.

(b)(4) [redacted]

8.6.1 QA/QC – Testing of Pipes

Berg's QA/QC program is implemented through its manufacturing procedure specification and quality plan. It is aligned to API Q1 (7th Ed.) and ISO 9001:2000. In practice, that means documented procedures and records, qualified personnel, calibrated test equipment, material and process traceability, nonconformance and corrective-action control, supplier oversight, and internal audits so inspection, testing, and release of pipe are managed under a certified quality management system.

As per Berg quality control test report [MTR – NPS30 – 386] [45] prior to release, pipe from each heat was subject to a complete QA/QC program covering identification, dimensions, NDE, pressure testing, and mechanical/metallurgical verification. Plate and wall thickness were confirmed, and traceability was established. The longitudinal seam underwent automatic ultrasonic inspection, accompanied by real-time digital radiography at the pipe ends and targeted locations, as well as pipe-body ultrasonic testing for laminations or linear indications. Every joint was hydrostatically tested with charted pressure/hold. Mechanical qualification included transverse pipe-body tensile tests, transverse weld-tensile tests, and guided bend tests of the seam. Fracture toughness and metallurgy were verified through Charpy impact testing on the pipe body, weld, and HAZ, as well as drop-weight tear tests (DWTT) and Vickers hardness traverses across the weld/HAZ/base metal. Product chemistry was confirmed against the specification. Only pipes that meet all acceptance criteria and documentation/traceability requirements were approved for shipment.

8.6.2 QA/QC Improvement Suggestions

Here we propose targeted QA/QC actions to close observed gaps in weld-geometry control, inspection coverage, and specification alignment. Below are some improvement suggestions

- For future pipeline procurement, it is recommended to implement the latest API 5L workmanship and repair provisions across the mill's MPS/ITP, and apply the most stringent requirement when API, purchaser (TES-PIPE-SAW-US) [39], or internal limits differ.
- Recommended to strengthen specifications, e.g., pipe end vs pipe mid-body assurance. Because current standards focus on visual/dimensional checks that are pipe end-focused, if any end inspection fails, it is recommended that sacrificial mid-length sectioning on that joint (and statistically on adjacent joints in the lot) be performed for macro-examination of the complete weld profile, including offset, peaking, fusion, and penetration.
- WPS/PQR qualifications may include characterization of the heat-affected zone (HAZ). Such a characterization may consider microstructural evaluation and J-R testing, including review of fractography.
- Utilize NDE techniques to inspect the pipe end and the pipe mid-body weld. Consider using a targeted destructive test to verify the effectiveness of NDE.
- Consider implementing a shop floor "mini-lab" capability for quick cut and etch macro examination by weld mill operators, which will enable proactive corrective actions. Suppose any indications are reported during the shop floor examination. In that case, it is recommended to perform mechanical/toughness checks (weld tensile, charpy/HAZ, hardness traverses) on representative samples to provide technical assurance beyond NDE.
- Focussed training of weld mill operators and NDE Inspectors on manufacturing seam weld defects and NDE interpretation is recommended. In addition, maintaining a shopfloor defect-part library (macro sections, photos, and digital examples) for calibration, onboarding, and competency checks will help to raise QA/QC awareness.
- Using continuous, automated digitized seam quality monitoring, data capture on the seam (weld-head position, heat input, wire/flux feed, travel speed, arc voltage/current, laser seam-tracker offset, and real-time waveform) alarm systems will allow operator to intervene and detect off spec radial offset.

8.7 Transportation

The Berg railcar banding procedure BPP-SOP-SHP-005 [46] has been developed in alignment with recognized industry standards to ensure the safe and reliable transportation of line pipe. Specifically, the procedure references API Specification 5L specification for line pipe dunnage requirements, and the AAR Open Top Loading Rules Manual for mandatory guidelines governing the securement and loading of pipe on open-top railcars. Together, these specifications provide the technical foundation for BPP-SOP-SHP-005, ensuring that Berg's banding and loading practices meet both pipeline industry requirements and railroad regulatory standards.

Recognizing the unique susceptibility of thin-wall, large-diameter line pipe to transit fatigue, the American Petroleum Institute (API) developed API recommended practice 5L1 (Railroad Transportation of Line Pipe) in the 1960s [40]. This recommended practice is explicitly written as supplementary to AAR rules as AAR rules govern universally, while API 5L1 addresses pipeline specific issues such as limiting static and cyclic stresses, bearing strip spacing, and end protection. The foreword note of API 5L1 states that "if any recommendations conflict with AAR loading practices, those of AAR shall govern."

Table 20 provides summary of transportation requirements listed in AAR and API standards. Given that the Keystone pipeline has a nominal diameter of 30 inches and a wall thickness of 0.386 inches, the D/t ratio is > 50. According to API RP 5L1, Section 4.1, this requires that both static and dynamic forces acting on the pipe during rail shipment be carefully evaluated, in order to minimize the risk of longitudinal fatigue cracks. Therefore, allowable static load stresses must be calculated, incorporating a factor to account for expected cyclic stresses, to ensure transportation-induced fatigue is avoided.

The concept of transit fatigue was included in the code, leading to stress limits (e.g. 16,000 psi static stress for bottom-row pipe during rail shipment). Later, API 5LT (2012) extended these learnings to truck transportation, addressing trailer conditions, bearing strips, separator strips, overhang restrictions, and handling QA/QC requirements. API 5LT is not applicable to the current key stone pipeline project as the order is placed in 2008 when the specification doesn't exist.

Table 20: Summary of transportation requirements listed in AAR and API 5L1 standards [47]

Aspect	AAR Open Top Loading Rules Manual (OTLRM, Sec. 2 – Metal Products incl. Pipe)	API RP 5L1 (Railroad Transportation of Line Pipe)	API RP 5LT (Truck Transportation of Line Pipe) only applicable to future projects
Scope	Section 2: Rules for Loading Metal Products, Including Pipe (p. iii–iv, 2017 ed.)	Clause 1.1, p. 1 – Scope: applies to API 5L line pipe ≥ 2⅜ in. OD, longer than single random	Clause 1, p. 1 – Scope: applies to line pipe transported on trucks/trailers
Legal Status	General Rules, Sec. 1 (p. iii) – Mandatory in U.S. rail service	Clause 1.2, p. 1 – API rules are supplementary; AAR governs in case of conflict	Foreword (p. iii), "Shall = minimum requirement; Should = recommendation"
Car/Trailer Condition	General Rules Sec. 1 (p. iii), "cars must be structurally sound, free of defects"	Clause 3.1, p. 2 – Railcars must be free of protrusions, debris, bent/torn parts	Clause 5, p. 2 Trailer condition requirements

Aspect	AAR Open Top Loading Rules Manual (OTLRM, Sec. 2 – Metal Products incl. Pipe)	API RP 5L1 (Railroad Transportation of Line Pipe)	API RP 5LT (Truck Transportation of Line Pipe) only applicable to future projects
Bearing Strips	Sec. 2 – Pipe loading figs. (e.g., Fig. 136, p. vii) approved bearing piece designs	Clause 3.2 & Sec. 4, p. 2–3 Bearing strips; Clause 4.3, p. 3 – Max static load stress (D/t ≥ 50)	Clause 8, p. 3 Bearing strips: number, positioning, blocking, materials
Separator Strips	General Rules Sec. 1, approved restraint components (p. iii)	Clause 3.3, p. 2 – Separator strips between pipe layers	Clause 9, p. 4 Separator strips: location & materials
Stacking / Geometry	Sec. 2 – Pipe figures (e.g., Fig. 124–136, p. vii) stacking geometry	Sec. 4, p. 2–3 Static stress & geometry; Transit fatigue discussion (Foreword, p. iii)	Clause 10, p. 4 Overhang & stacking limitations
Tie-Downs / Banding	Sec. 2 Pipe figures (e.g., Fig. 147-A, 153, 160, p. vii) band anchors/chain tie-downs	Clause 3.7, p. 2 Banding and tying down requirements	Clause 12, p. 4 Positioning & tie-downs for SAWL/COWL pipe
Inspection / QA-QC	Sec. 1 General Rules (p. iii) inspection responsibility of shipper & carrier	Clause 3.8, p. 2 Inspection before and after shipment	Clause 5 & 12.1, p. 2–4 Inspection of trailers and pipe; reject damaged joints
Fatigue / Stress	Not pipe-specific general safe loading	Foreword (p. iii) & Clause 4, p. 2–3 Transit fatigue, cyclic stresses; Max static stress ≈16,000 psi	Clause 7 & 11, p. 2–4 Containerized loads, handling equipment; based on PRCI truck vibration studies
Seam weld orientation	Remains silent	weld seams should be oriented to avoid contact with steel banding straps.	weld seams shall be oriented to avoid contact with steel banding straps.

8.7.1 QA/QC During Transporation

Modern transportation QA/QC practices, as outlined in the AAR OTLRM [47]and the API Recommended Practices 5L1 (railroad) [40]and 5LT (truck) [48], are designed to minimize the risk of shipping-induced damage to line pipe. These include inspection of railcars and trailers to ensure they are free from protrusions, debris, or swayback that could damage the pipe; verification of bearing strip material, size, and placement in line with API 5L1 stress control requirements; and use of separator strips to prevent coating abrasion between adjacent joints. Proper tie-downs and banding methods specified in AAR and API standards are applied to prevent shifting during transit. Additionally, QA/QC requires inspection of pipe before loading and after delivery, with removal or rejection of any damaged joints, ensuring integrity assurance is maintained throughout transportation.

8.7.2 Staff Interview Perspectives

In discussion with the TPI Contractor, who managed overall QA/QC and third-party inspection (TPI) activities for TC Energy, it was confirmed that all applicable transportation guidelines were followed for the shipment of the subject pipe. The TPI Contractor emphasized that seam weld orientation is controlled so there is no possibility of weld-to-weld contact nor contacting dunnage during transportation, and that this remains standard practice whether pipe is shipped by truck or rail.

TPI further noted that the AAR Open Top Loading Rules govern rail transportation, and as such, railroads will not accept cars unless AAR requirements are met. While TC Energy and PHMSA special permit specifies compliance with API RP 5L1, Berg followed AAR practices, which supersede in the context of rail shipments. Importantly, AAR does not provide requirements regarding seam weld orientation; therefore, there is no conflict between AAR and API 5L1 on this matter. TPI stressed that weld-to-weld or weld-to-dunnage contact will not occur under standard loading practices, and that there is no inconsistency in whether Berg applied AAR or API 5L1 procedures. This assurance reflects the application of proper bearing strips, separator strips, and banding arrangements in compliance with AAR and API 5LT transportation standards.

8.8 Conclusions and Recommendations

8.8.1 Conclusions

1. Based on manufacturing surveillance quality control reports, the DSAW pipes are compliant with API 5L 43rd edition, and meet all of the TC energy specifications.
2. The pipe microstructure consisted of fine-grained ferrite and pearlite, typical of low-carbon, low-alloy line-pipe steel. The weld microstructure was free of internal defects. The chemical composition, tensile properties, and impact toughness of both the pipe body and the seam weld complied with the applicable requirements of API 5L, 43rd Edition, for Grade X70 and the TC project specifications. A microhardness survey showed uniform hardness across the base metal, seam weld, and HAZ, with values typical of X70 carbon steel.
3. The seam weld HAZ must be evaluated as part of the WPS/PQR qualification, which may require detailed characterization of the HAZ. This characterization can include microstructural examination, J-R testing, and fractographic analysis.
4. Since the current inspection is limited to the ends of the pipe this cannot provide assurance to seam geometry; off-spec radial offset along the pipe body which can easily go undetected. To close this gap, manufacturers require full-length automated UT of the weld seam and explore continuous real-time NDE techniques for detection of out of spec weld geometry should be prioritized.
5. Berg followed the AAR OLTRM guidelines, while the purchase agreement from TC Energy required compliance with API RP 5L1 [48]. Because API RP 5L1 defers to AAR requirements in the event of any conflict, Berg's adherence to AAR was inherently consistent with the API RP 5L.
6. Based on feedback from staff interviews, it was confirmed that during transportation seam weld orientation is controlled during transportation to ensure there is no possibility of weld contact (pipe or supports), and that this control is maintained as a standard practice for both truck and rail shipments.

8.8.2 Recommendations

1. It is recommended exploration of improving or implementing continuous real-time NDE for detection of seam weld geometry with pipe mills is explored as a first step before any destructive testing is considered.
2. If weld radial offset is detected at a pipe ends, consider destructive verification. Because offset is only reliably visible at the ends, any detection shall trigger cutting a short ring from that joint and preparing macro-etched cross-sections to measure radial offset, offseam weld, geometric deviations to confirm weld fusion/penetration. Accept/reject against API 5L / TES / BERG limits; if nonconformance is detected, consider sectioning to mid-length and quarantine the lot for 100% screening. It is recommended that exploration of improving or implementing continuous real-time NDE for the detection of seam weld geometry with pipe mills shall be explored first.
3. Training of weld mill operators and inspection personnel on dimensional seam defects (radial offset/hi-lo, peaking/ “flat spots and peaks,” lateral offset, reinforcement/undercut) will increase awareness. Maintain a controlled defect part library (macro etched coupons, macro etched cross sections, weld profiles a) to train weld-mill operators and inspectors and to support periodic competency checks. Consider shop-floor mini labs (with quick cut, etch, and basic hardness capability, as well as HAZ evaluation) or quick turnaround from internal labs so that questionable weld samples can be validated at the source rather than being discovered later during final inspection.
4. Tighten traceability of geometry inspections. Require the mill to record measured values (offset, peaking, bead height), locations, inspector ID, and tie them to unique pipe numbers/heat/shift so findings are auditable.

9 Inline Inspection

Throughout the history of the KS6 segment, multiple inline inspection tools have been run through the pipeline. They are summarized below in Table 21.

Table 21: Summary of inspection runs

ILI Description	Technology	Run Date	Key Findings
(b)(4)	MFL + Caliper (Metal Loss)	Mar. 2012	Small Internal/External ML
	MFL + Caliper (Metal Loss)	May, 2016	Small Internal/External ML
	Ultrasonic Crack	Dec. 2017	2 Crack like; 1 Weld Anomaly; 45 Geometry Digs verified grinds on the weld.
	MFL+SMFL+LFMFL+Caliper (Metal Loss)	Jan. 2018	Small Internal/External ML
	Ultrasonic Crack	April 2020	Detected 3 axial colonies and 10 axial cracks One excavation 28% was a weld defect
	Ultrasonic Crack	Sept 2020	Detected 3 axial cracks and 4 axial crack colonies
	Caliper	Oct. 2021	
	Ultrasonic Wall (Metal Loss)	July 2021	Internal and External ML were identified
	Ultrasonic Crack Circum.	Nov 2023	7 crack-like anomalies along the GW

South Bow has run numerous inspection tools through the KS6 segment. There are the typical and traditional MFL and Caliper runs that have been conducted over time, focusing on metal loss, deformation, or mechanical damage. They have been effectively managing these threats, and these will not be discussed in further detail here.

Ultrasonic crack detection technology utilizes an incident angle of approximately 17 degrees through the oil (coupling) medium to deliver a 45-degree angle through the steel, allowing for the location of internal and external cracks in the pipe wall at different time steps. This concept is shown below in the Figure 84 from the literature. If there are no cracks, there will be no echo back from the refracted wave. This is the concept of all tools; the challenge is in redundancy, interpretation, and separating signal from noise.

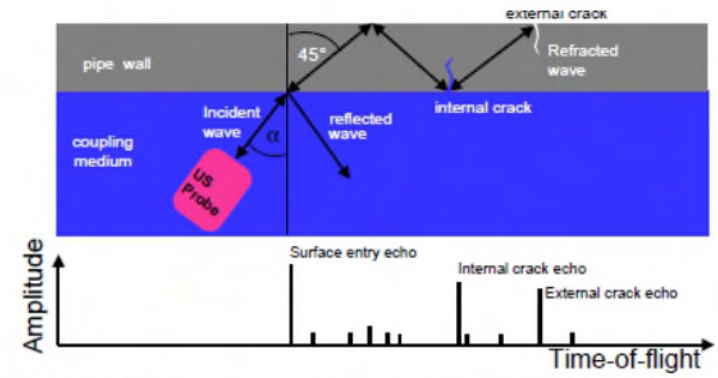

Figure 4: The principle arrangement for ultrasonic crack detection. Sound waves will travel through the pipe wall at an angle close to 45 °.

Figure 84: Ultrasonic wave through steel at 45°

The UT technology is amongst the best for crack detection, and over the years, since the 1990s, it has successfully identified, sized, and consequently mitigated cracks throughout the pipeline industry. They have been very successful with SCC and other forms of cracking, including fatigue cracks, selective seam weld cracks, and many others.

The focus of the discussion here are on the crack ILI runs performed to detect axially oriented cracks. South Bow utilized CD+ run in 2017 before the 2019 Edinburg incident, and two crack ILI runs using [redacted] and [redacted] in April and September 2020, respectively. The 2017 CD+ run identified three anomalies, with the deepest being recognized as a weld anomaly, which also had the highest depth of 23% and a length of 13.45 inches. The excavation data indicated that the anomaly was a mill grind; there was no crack.

Most importantly, South Bow also conducted verification runs along with the inspections in April and September 2020. The purpose of the verification runs was to assess the impact of these anomalous weld geometries on crack detection and sizing.

South Bow created correlation spools that were evaluated on KS5 as part of the [redacted] tool run in April 2020. The peaking angle appeared to approach approximately 21 degrees, which is higher than noted in the MP 171 failure. There were 25 individual features, including both EDM and weld-induced methods. Another spool had defects introduced through thermal fatigue, around 10 individual features. Since two features were inadvertently collocated, the total defect population was 34.

The results were impressive with [redacted] there was 100% POD for defects within the tool specifications. Four out of nine outside of the tool specification went undetected. Two were less than 10% in depth or less than 1 in., and two were adjacent to the girth weld. These results provide significant confidence in the technologies. Similarly, the [redacted] tool successfully detected all anomalies in the correlation spools. A UT simulation was also conducted by [redacted] giving confidence in the approach.

The [redacted] run in April 2020 revealed 13 crack-like anomalies, many of which appear to be internal. The deepest one, with a depth of 28% and a length of 7.9 inches, was excavated and found to be an innocuous weld grind.

The [redacted] run in September 2020 was performed to augment the April 2020 [redacted] run. A review of the specifications revealed that the [redacted] gave better depth sizing than [redacted] for anomalies with a radial tilt angle between 12 and 45 degrees. The [redacted] tool revealed seven crack anomalies, of which three were associated with the seam. Further, the [redacted] downgraded five of the eight cracks to seam weld inhomogeneities. Three remaining cracks were excavated, including the deepest seam feature, at 23.5% and 11 in. in length. No anomalies were found with NDE following excavation. (b)(4) [redacted]

Following the two UT Crack tool runs in 2020, which successfully located the cracks in the correlation spools and didn't identify any crack-like indications in KS6, (b)(4) [redacted]

The MP 171 rupture through the fatigue crack conflicted with the 2020 UT data. The rupture location exhibited no signal, no crack indications in the (b)(4) [redacted] data. The crack defect length was approximately 8 inches, and its depth was estimated to be between 28% and 50% of the wall thickness, ranging from 0.11 inches (2.7 mm) to 0.19 inches (4.8 mm). (b)(4) [redacted]

KS6 has had three different Ultrasonic shear wave tool runs, and none of them identified or obtained a signal at the rupture location. The weld peaking angle of 15 degrees affects the refracted wave angle in the pipe steel, causing a deviation from the desired 45 degrees, which consequently reduces the amplitude of the reflected signal. Additionally, the radial tilt angle of the crack as it intersects the plate surface was approximately 10 to 15 degrees, which also reduces the amplitude of the reflected signal. This is in contrast to the correlation run but consistent with the UT simulation modeling. The inconsistency should be investigated and understood; it doesn't impact the RCFA, but it is essential for the successful application of these technologies.

The proper solution may involve the possible use of a PAUT ILI tool that focuses on the peaking seam issue. The PAUT ILI tool offers two to three different incident angles, with the ability to create a refracted angle that detects the HAZ crack in a peaked weld. These tools are available in other sizes; (b)(4) [redacted]

Any such technology should be verified using correlation spools, similar to the tests conducted in 2020. First, as before, South Bow should create peaking welds of 12 to 15 degrees based on MP 171 and Edinburg failures. However, Blade would recommend utilizing fatigue cracks, especially for peaking welds. Fatigue cracks can be generated in these welds using either pressure cycles or displacement perpendicular to the weld. The EDM notches, weld anomalies, and thermal fatigue anomalies may not accurately reflect the fatigue crack morphology, which may explain the inconsistency between the correlation tests and the field performance. This is just a hypothesis that should be verified. Additional review is necessary to rationalize these results.

South Bow has developed an approach in collaboration with (b)(4) [redacted] which utilizes a UT compression wave tool to identify peaking weld angles. The algorithm appears to be quite advanced and has been further supported by field data. This approach should be considered to identify welds that exhibit peaking in the range of 12 to 15 degrees, consistent with the failures at Fort Ransom and Edinburg. An FEA model of the weld can be utilized to establish the angles, weld bead offset, and plate offset. Utilizing other ILI tools and technology, perhaps targeted excavation to assess cracking. There is further discussion in Section 11.4.

South Bow should consider magnetic technologies, such as circumferential MFL (CMFL), to locate cracks. Blade conducted a preliminary FEA analysis of a crack with 78% depth, length of 8 inches. Crack was assumed to be elliptical, and subject to 1440 psi pressure. The crack mouth opening was estimated to be approximately 0.0506 inches (1.28 mm) which is higher than 0.1 mm crack width requirements, shown in Figure 85. CMFL tools may also have issues with peaking, and should be evaluated. It presents an alternative that may be worth pursuing. Additional FEA modeling to assess the CMOD as a function of pressure, crack depth, and length should inform the decision-making process.

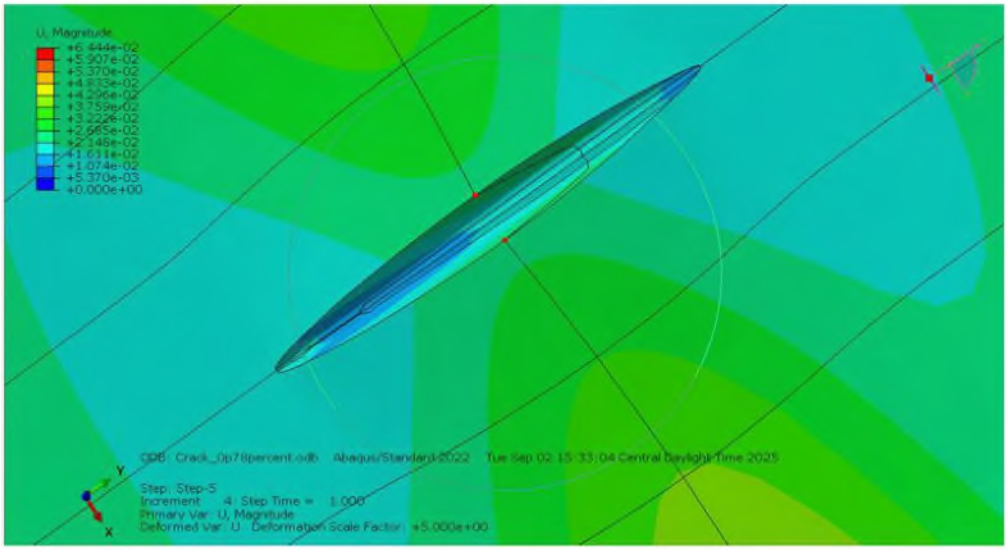

Figure 85: CMOD for an 8 in crack at 1440 psi and 78% depth.

A correlation spool with fatigue cracks should be utilized to assess these technologies. Since POD is the focus, such a technology may provide value. However, additional work is necessary to qualify such technologies.

9.1 Summary

1. South Bow conducted three different axial crack ILI tools through the KS6 segment. None of them detected crack-like signals in the rupture region. It was estimated that the cracks at the rupture location were approximately 28% to 50% in 2020, during the last two axial crack inspection runs.
2. The correlation run exhibited POD approaching 100% for the last two UT shear wave tools, (b)(4) and (b)(4) The cause for the inconsistency between the correlation spool and the 2020 inspection runs should be investigated.
3. South Bow, in collaboration with (b)(4) has developed an application utilizing the UT compression wave tool to identify roof topping locations. These should be further refined and could be used for locating sites where there may be HAZ cracks.
4. Magnetic technologies should be further explored for identifying roof topping and detecting cracks. Preliminary FEA modeling indicates a crack mouth opening that is far greater than the 0.1 mm limit for CMFL tools.

10 Discussion and Key Conclusions

The overall approach taken for the RCA required a detailed understanding of the mechanism of cracking, seam weld manufacturing, double jointed pipe transportation, ILI, fracture and fatigue analysis, metallurgical analysis, standards and procedures, the Edinburg failure, integrating all the information, and finally the Apollo RCA process to identify root causes and solutions.

The pipeline experienced around 546 MOP cycles in the 15 years of operations. A preliminary review, considering it involves high-cycle fatigue (hoop stress less than yield), suggests that the number of cycles is inadequate to initiate and propagate a crack to failure.

The first step is to understand the mechanism of crack initiation and propagation, and, more importantly, to locate evidence that supports this interpretation. Blade pursued two approaches: one focused on modeling and the other on fractographic evidence.

A modeling approach was employed to quantify the number of operating pressure cycles required to initiate and propagate a crack. To assess crack initiation, Blade utilized a fundamental model known as the Smith-Watson-Topper model. An FEA model of the weld (with peaking and bead offset-simulating rupture location) was used to determine the strain range resulting from pressure cycles. The strain range from the FEA was utilized in SWT; crack initiation through pressure cycles would require around 130 to 478 MOP pressure cycles. Next, a fatigue crack growth analysis was completed, using the highest FCGR data from API 579 (electrochemical hydrogen generation). One would need a pre-existing crack depth of around 12% for the rupture to occur in 2025. Based on this, it is unlikely that the crack initiated and grew to failure solely due to pressure cycles.

Blade decided to explore fractographic evidence to see if there is support for such an interpretation. A more detailed examination of the fractographic data, conducted using a scanning electron microscope (SEM), revealed two distinct regions in the fracture surface. Closer to the ID, the nature of the fatigue fracture surface morphology was like that of fatigue in air, with clear indications of striations. As one traverses the fracture surface from ID to OD, at approximately 5 to 10% of the crack depth, the fracture surface transitions to a more brittle nature. Further away from the ID, beyond 5 to 10% depth, the fracture exhibits increasing brittleness. The fractographic data indicate a period during which fatigue may have occurred in air (ID to around 10% wall thickness). In contrast, there was a period during which hydrogen played a role in the fatigue process (10% to 78% wall).

The fractographic evidence reveals two distinct crack propagation mechanisms on the fracture surface, one occurring in air and the other in a more embrittling environment. The environmental factor considered most likely was hydrogen, as the fracture surface exhibits cleavage and quasi-cleavage.

Blade undertook three approaches to verifying the hydrogen interpretation. The first one involved quantifying the hydrogen in the weld region of the pipe used for transporting crude oil, as well as the pipe in inventory that had never been exposed to crude oil. There was a difference between the two welds; the pipe used for transportation showed higher levels of hydrogen. The second approach involved quantifying the scale on the fracture surface, which was verified to be Iron sulfide and Iron sulfate. This implies that hydrogen sulfide may have been present locally, which could lead to hydrogen embrittlement of carbon steel. The third approach involved using a representative concentration of the oil and evaluating it using the thermodynamic tool OLI. Using 0.2% water in the oil, OLI estimated that up to 18 ppm of H_2S may be present in the water phase.

The fusion bond epoxy coating was intact in the vicinity and the region of the failure. Consequently, cathodic currents would not reach the pipe surface. Therefore, CP could not have contributed any local hydrogen uptake in the pipeline.

By integrating crack modeling, fractographic evidence, and hydrogen environment data, the following key conclusions are derived.

- Crack propagation in the crude oil environment exhibits a hydrogen-enhanced fatigue crack growth rate due to the cleavage and quasi-cleavage fractography. The HAZ microstructure appears to be compromised as indicated by fractographic data from J-R fracture testing at -5 °C. But the fatigue pre-cracking fractographic data indicate no cleavage indications. Consequently, the presence of cleavage and quasi-cleavage in the rupture sample indicates a hydrogen-enhanced fatigue crack propagation.
- Consequently, the region closer to the ID, where there is air fatigue type fractography, should have occurred in an environment other than the crude oil. The only other possible mechanism is fatigue crack initiation and propagation during transportation from the Berg facility to North Dakota, which is approximately 1,605 miles by rail and 27 miles by road.
- There is a high possibility that the crack initiated and propagated to around 12% during transit. RSI during the Edinburg failure assessed the weld with peaking and plate offset, and demonstrated that transit fatigue cracks are feasible.

The MP 171 weld, with peaking and bead offset, meets all the API 5L 43rd edition requirements. Further, Berg appeared to have followed all relevant transportation guidelines. The enhanced stress concentration factor in the weld toe region directly contributed to the initiation and subsequent growth of the crack.

Following the Edinburg rupture, South Bow implemented two key recommendations, amongst others. The cyclic pressure loads were further reduced. Also, South Bow conducted two crack ILI inspection runs in 2020. Despite successful verification runs using artificial cracks, the 2020 crack ILI inspections did not register any crack-like signals at the rupture locations, (b)(4) [redacted]
(b)(4) [redacted]

10.1 Future Work

This is a summary of possible future work (not ILI-related) that would enhance the understanding of the underlying mechanism of cracking. These recommendations are not necessary to conclude the current RCA.

- (b)(4) [redacted]
- Characterize the HAZ microstructure in terms of phase fractions using techniques such as EBSD and TEM.
- Quantify the Coffin-Manson parameters for the HAZ, and quantify fatigue crack initiation in the HAZ.
- Quantify fatigue crack growth in a hydrogen-generating environment in the various microstructures of the HAZ.
- Establish DBTT for the HAZ, and perform high-fidelity J-R testing at operating temperatures.

11 Root Cause Analysis

A team consisting of Blade investigators involved in all aspects of the RCA project was assembled to execute the structured Apollo RCA.

Following the completion of analysis, modeling, review, and additional metallurgical laboratory work, a two-day root cause analysis workshop was conducted with Apollo RCA facilitator Fadi Rahal. The participants included the entire Blade team that had reviewed and analyzed the data. It included Ryan Milligan, Ken George, Janardhan Saithala, Richard McGregor, and Ravi Krishnamurthy. The results of the RCA are presented in this section of the report.

11.1 Root Cause Analysis Process Background

A root cause analysis (RCA) is a systematic process used for identifying the root causes of problems or events and defining methods for responding to and preventing them. In other words, this process helps companies learn from past events and develop plans to improve safety and reliability. The goal of an RCA is to analyze problems or events to identify:

- What happened.
- How it happened.
- Why it happened.
- What actions are needed to prevent reoccurrence.

There are many different methods and philosophies for conducting an RCA, such as 5-Why's, Fish-Bone Diagram, Fault Tree, Management Oversight, and Risk Tree Analysis, depending on the industry and type of problems being investigated. However, most of them use preconceived or pre-defined categories of causes.

Blade selected the Apollo Root Cause Analysis (ARCA) approach because it is a structured, evidenced-based process that makes no assumptions about possible causes [49]. The ARCA companion RealityCharting software was used to develop a cause-and-effect chart, identify the root causes, and develop solutions. This methodology has been used in the energy, chemical, and aerospace industries.

The ARCA process starts with defining a primary effect, that is, the effect that should be prevented from occurring. The next step is to determine the causes of the primary effect. An *effect* has at least two causes in the form of conditions and actions, and together they become a causal set (Figure 86). Conditional causes are static causes that exist over time prior to the action.

Action causes are causes that interact with conditions to cause an effect. In other words, the condition must already exist for the action to cause the effect, and the condition and the action must exist at the same time for the effect to occur. For example, think of a fire as an effect. The conditions (i.e., the static causes) for that fire to happen would be a source of oxygen and fuel. The action (i.e., what interacts with the conditions) for that fire to happen would be the addition of a heat source. The action plus the conditions would result in a fire, and the absence of any of the conditions would not result in a fire regardless of the action.

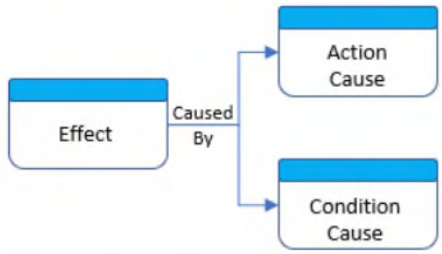

Figure 86: Causal set

Next, the question *what was this caused by?* or *why did this happen?* is asked for each of the action and condition causes. The causes in essence, become effects, and new action and condition causes are determined for each effect. This process of continuously asking what or why and determining causes for each effect is repeated and develops into a cause path until an end point is reached (Figure 87). A valid end point is defined as an effect that is caused by a desired condition (e.g., the pursuit of a goal), a lack of control (e.g., a legal requirement), or some other more relevant or productive cause path. During this process, the evidence supporting each cause must be identified.

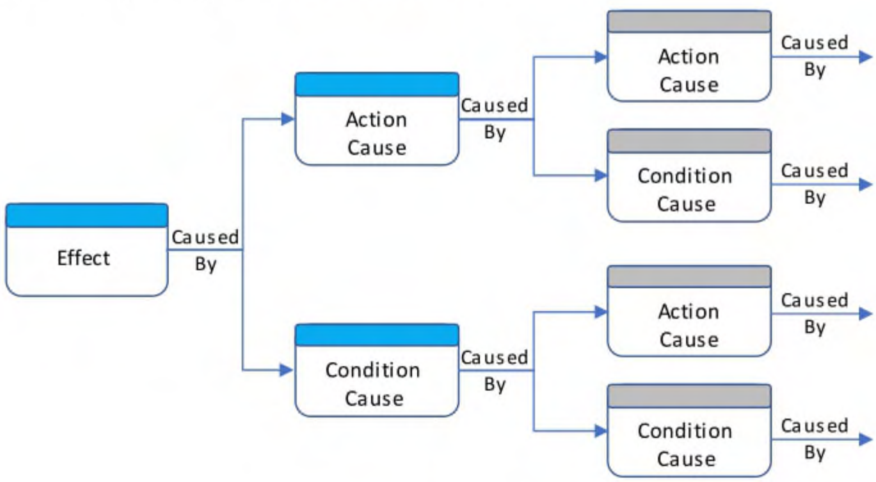

Figure 87: Casual flowchart development

When the causal flowchart is complete, the root causes are identified and solutions to mitigate or prevent them are developed. The criteria for developing solutions are:

- Preventing recurrence
- Being within one's control
- Meeting one's goals and objectives
- Preventing other problems

11.2 Root Cause Analysis Results

The total result of the Apollo RCA is provided in Appendix A. Each element of the RCA result is discussed below.

The first step in the RCA process was to determine the primary effect of April 8, 2025, when the KS6 pipeline ruptured downstream of the Fort Ransom pump station. When the pipeline ruptured, liquid hydrocarbon escaped into the surrounding area. Within 2 minutes, isolation of the ruptured section was initiated by remote control and locally by field personnel.

The RCA effort is focused on defining the primary effect and what could have been done to mitigate it. Further, the intent of identifying root causes and implementable solutions is to prevent the recurrence of similar pipeline integrity issues on the Berg pipe in the Keystone pipeline system.

Figure 88 shows the primary effect associated with the causes. The MP 171 Rupture is the primary cause. It was caused by Oil flowing at [redacted] kPa), the Pipeline was transporting hydrocarbon liquid, and the crack along the weld seam reached a critical crack size.

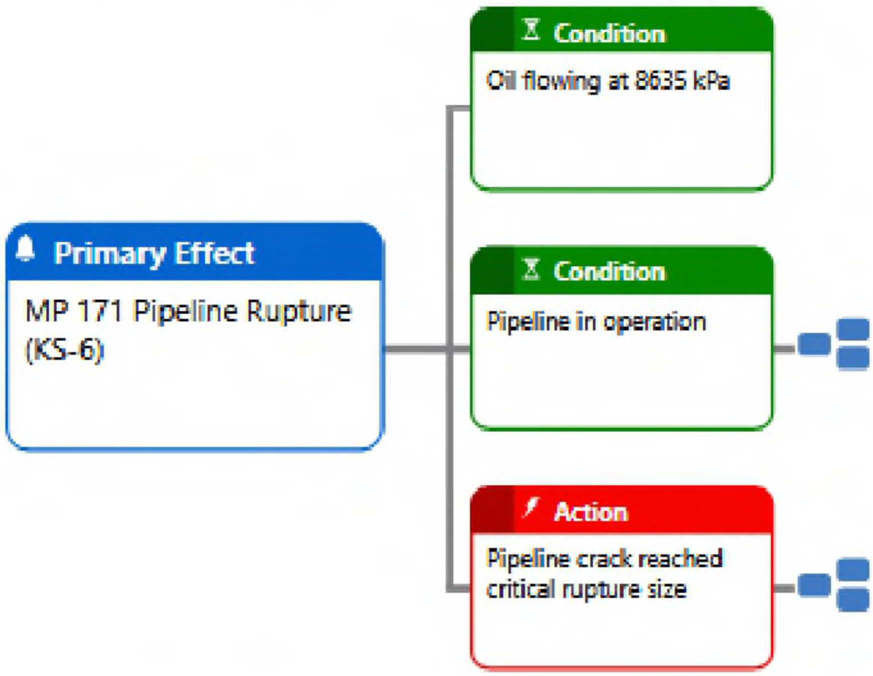

Figure 88: Primary Effect with associated causes

The oil flowing at 1252 psig (8635 kPa) is terminated as a desired condition. However, the Pipeline in operation is continued further. The cause for the pipeline to be in operation was due to four different causes as shown below in Figure 89:

- 2012 [redacted] baseline inspection.
- PHMSA requirement for a baseline inspection.
- Pipeline is required to transport crude oil
- Pipeline filled with oil in 2010
- Baseline caliper inspection run was completed

Except for the pipeline filled with oil, the other causes are terminated.

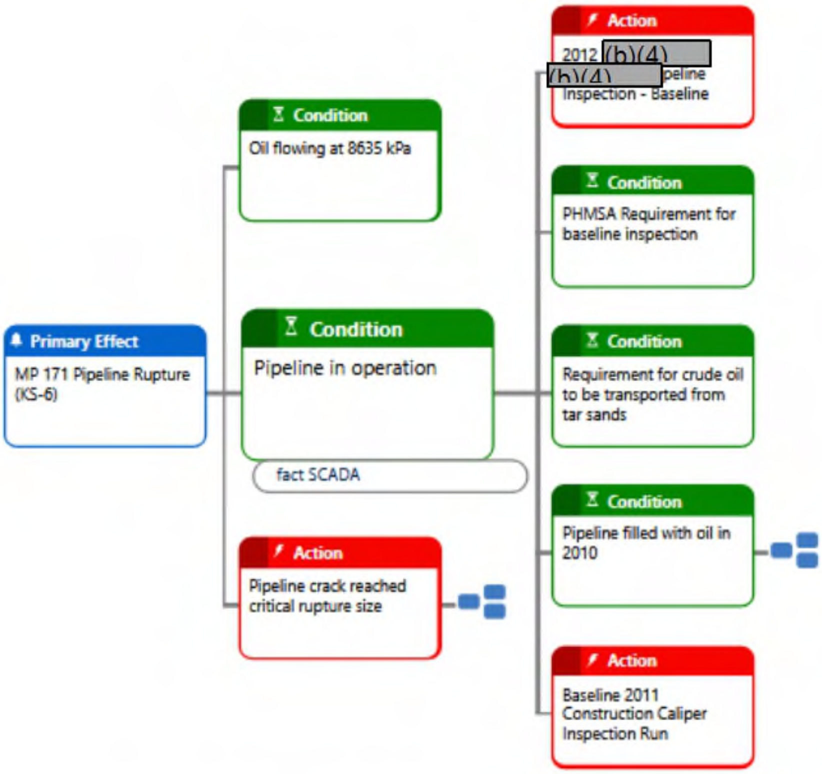

Figure 89: Causes for the pipeline in operation

The pipe was manufactured in 2008, pipeline constructed between 2008 and 2010, and consequently required transportation by rail for the first 1605 miles and then by truck for the final 27 miles. The causes, as shown in Figure 90 :

- TC Energy managed the pipeline, and it was constructed. This is terminated as a desired condition.
- Pipe was transported by rail/road. This occurred because Berg manufactured the pipe to the API 5L 2004 edition and TC specification, TES-PIPE-SAW-US. Berg manufactured the pipe in 2008. Furthermore, the pipe met the QA/QC requirements for the pipe.
- Berg followed AAR Open Top Loading Rules Manual 2007 train transportation guidelines. The Berg facility was over 1500 miles away, and rail transport was necessary. This is terminated as a desired condition.
- TC required API 5L1 for transportation. The API 5L1 guideline directs to the AAR transit guidelines in the event of a conflict between the two requirements. This is terminated as a desired condition.

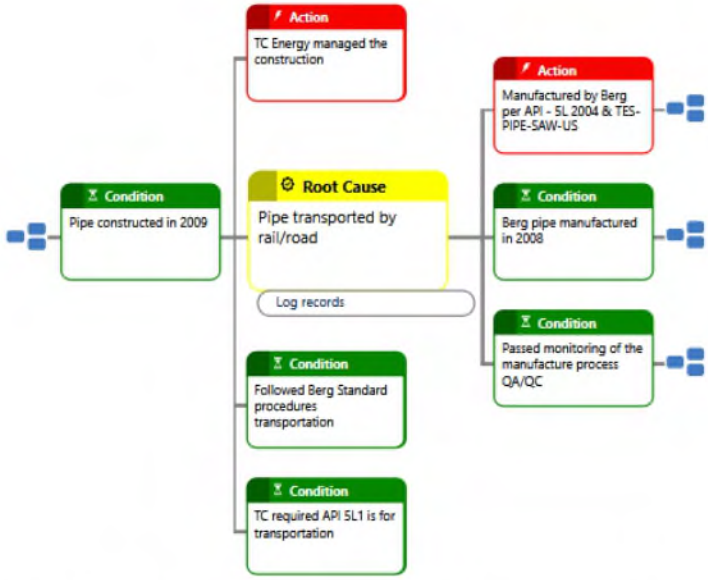

Figure 90: Causes for the pipe being transported by rail/road

The causes for Berg to manufacture the pipe to the API 5L 2004 and TC specification that was incorporated into the MPS were as follows, as shown in Figure 91:

- TC Operator and Berg agreed on the manufacturing specifications, and this was a termination point
- Manufacturing specifications are a regulatory requirement and an industry standard. This was also a desired condition.

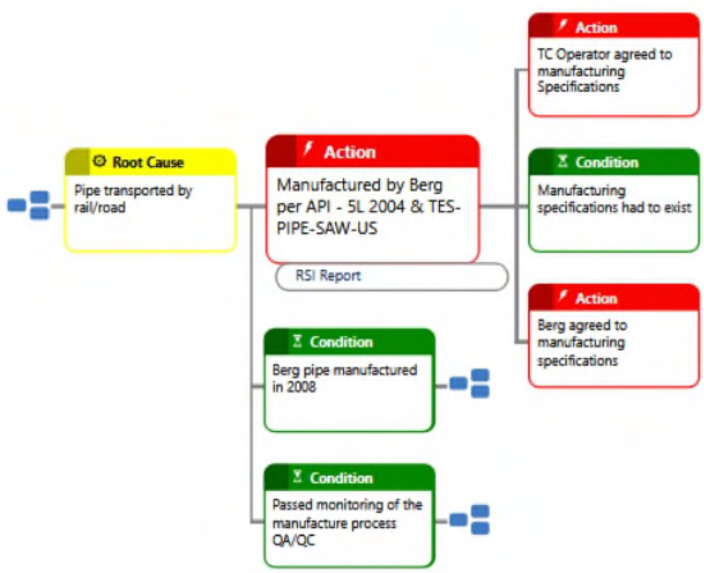

Figure 91: Causes for pipe to be manufactured to API 5L 2004 and TC specification

The causes for the Berg pipe manufactured in 2008 are shown in:

- The Heat-affected zone exhibited brittle behavior at -5 °C through the J-R testing. Cleavage was observed in the HAZ in both used and unused pipes. This is significant because any impact of the operating environment was absent in the unused pipe. The HAZ was clearly brittle before being put into operation. The manufacturing process is responsible for the brittleness.
- The seam weld consistently showed peaking and an out-of-line weld bead in the 2025 and 2019 failures.

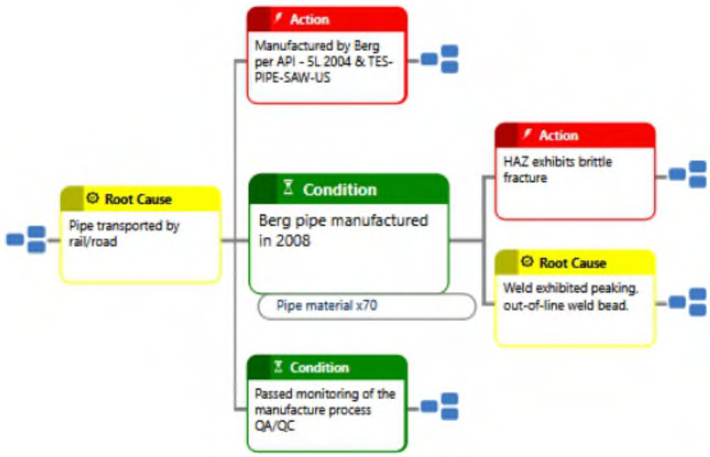

Figure 92: Causes for Berg pipe manufactured in 2008

The causes for HAZ exhibiting the brittle fracture are that the WPS/PQR did not evaluate HAZ. This wasn't part of the weld qualification. The other condition for the brittle fracture was that the WPS/PQR without the HAZ was qualified. Both these causes terminate as desired conditions. These are shown in Figure 93 .

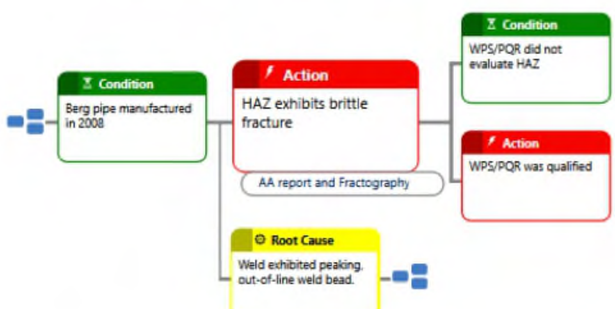

Figure 93: Causes for HAZ to exhibit brittle fracture

The causes of the weld exhibiting peaking and an out-of-line weld bead are that the pipe was DSAW welded by Berg, in accordance with API 5L 2004 requirements, and the failed weld did meet the TC peaking requirements. This causal set was terminated due to a desired condition and is summarized in Figure 94.

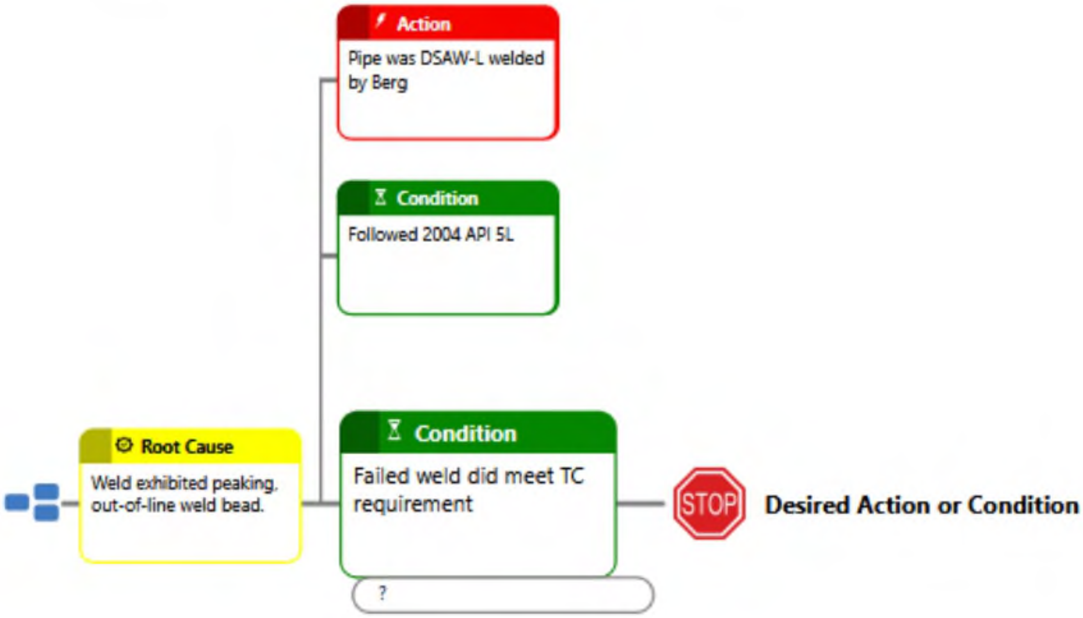

Figure 94: Causes for the weld issues

We shift our focus to the primary effect (Figure 88) and focus on the segment where the pipeline crack reached critical crack size. This is shown below in Figure 95. The causes for the crack being a critical crack size are two-fold:

- The subcritical crack propagated through fatigue in the hydrocarbon environment. Further, the cause for this propagation is the liquid hydrocarbon environment, and the fact that the September 2020 ILI (b)(4) did not detect this crack.
- The Heat-affected zone is susceptible to environmentally assisted fatigue crack growth.

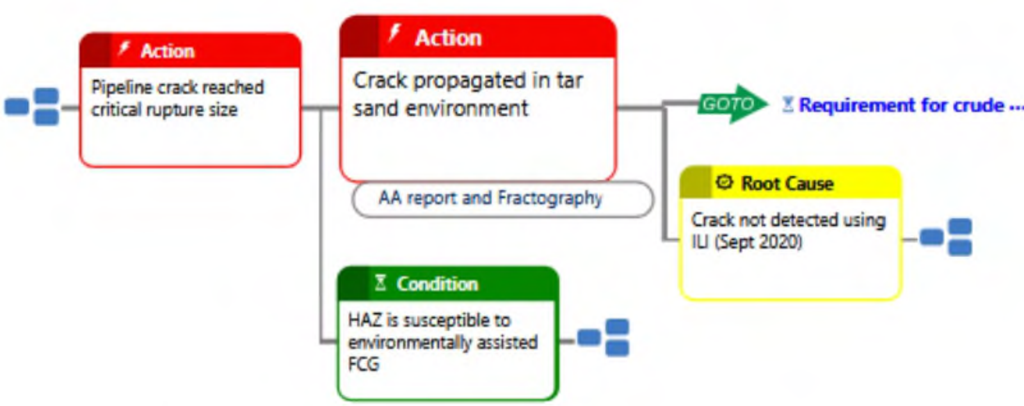

Figure 95: Causes associated with the crack reaching a critical crack size

The causes for the ILI not detecting the cracks are shown in Figure 96. The [redacted] was run in September 2020. The tool was inadequate for detecting cracks in the weld root radius due to weld peaking and a corresponding radial tilt of the crack. There was an extensive effort to verify the tool's efficacy; [redacted] The inadequacy was possibly due to the weld geometry not being adequately modeled experimentally as a combination of the peaking angle and radial tilt of the flaws, and/or the fatigue cracks not being simulated adequately, as shown in Figure 97. These are terminated due to a lack of control.

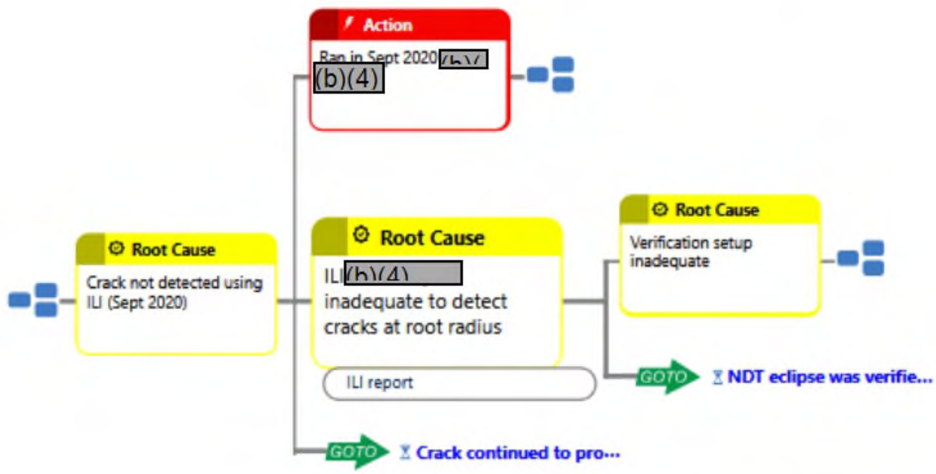

Figure 96: Causes for Sept. 2020 ILI not detecting the cracks

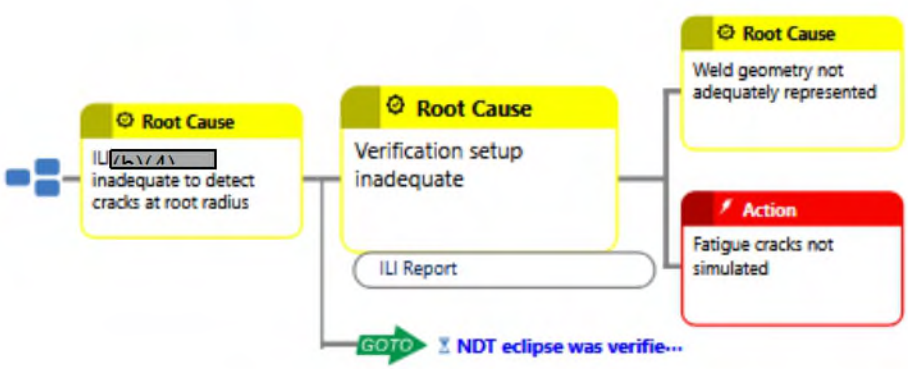

Figure 97: Causes for verification setup were inadequate.

The cause for running the September 2020 [redacted] is explored below in Figure 98. They include the following:

- No crack was detected using [redacted] tool in April 2020. A better tool and technology, the [redacted] that was verified was used.
- [redacted] went through a verification using correlation spools and simulation.

- [redacted] was considered inadequate for detecting cracks within peaking welds.
- Ran the [redacted] in April 2020 and didn't detect any seam weld cracks.

Further exploring why the crack wasn't detected in April 2020, [redacted] ILI was used, and alternate technologies and tools were assessed. [redacted]

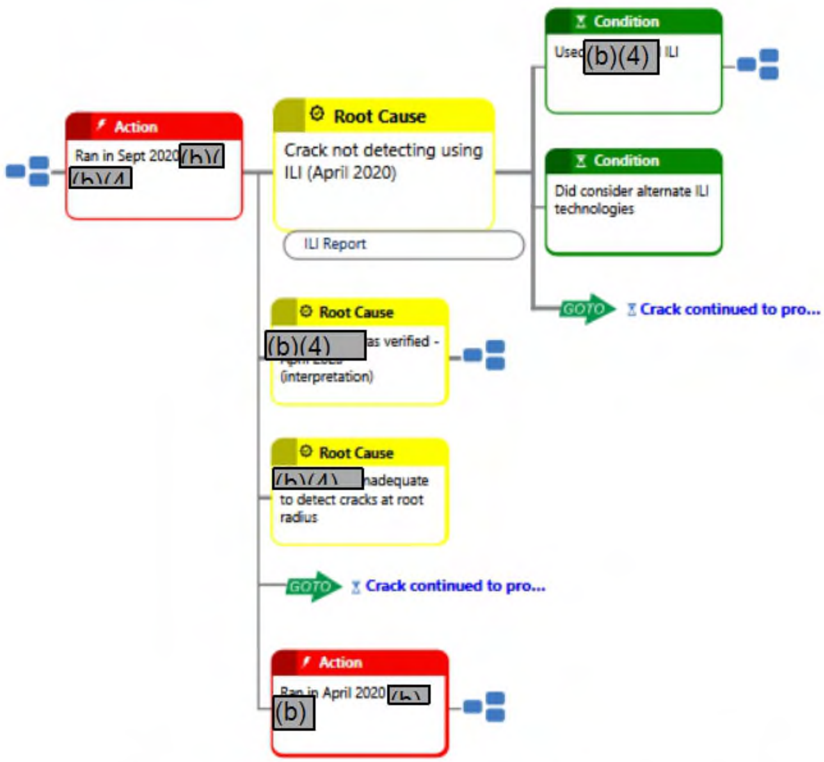

Figure 98: Causes for the September 2020 [redacted]

[redacted] was verified by [redacted] conducting a simulation, and TC Energy conducted tool verification using correlation spools. The correlation spools had artificial defects in a peaking weld that was manufactured. The decision was based on multiple inputs from modeling to tool verifications.

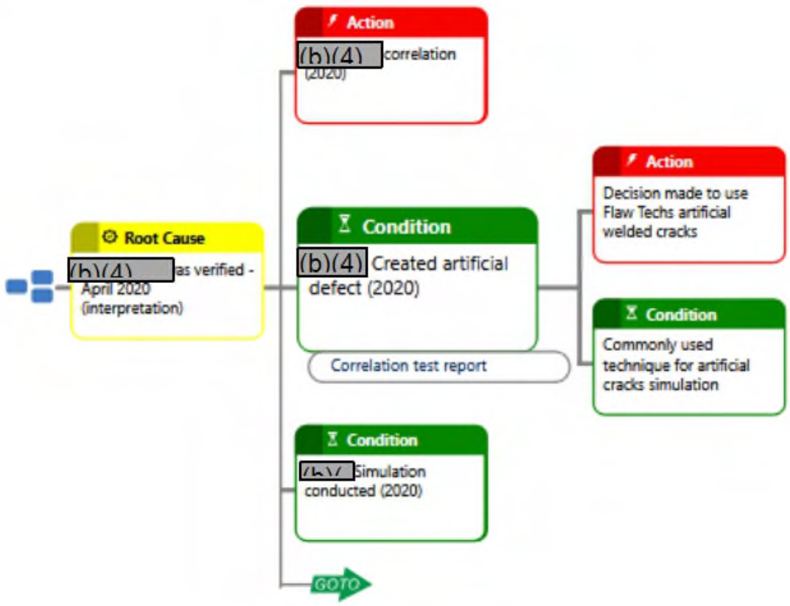

Figure 99: Causes for (b)(4) verification

The causes for running the April 2020 (b)(4) are summarized in Figure 100. The rationale for this would be as follows:

- No seam weld cracks were detected using the (b)(4) tool in 2017. The crack depth estimate was around 15% of wall thickness in 2017, and the tool was run in December of that year. Furthermore, the (b)(4) tool was inadequate to detect the cracks at the root radius.
- The other cause was that the crack continued to propagate.

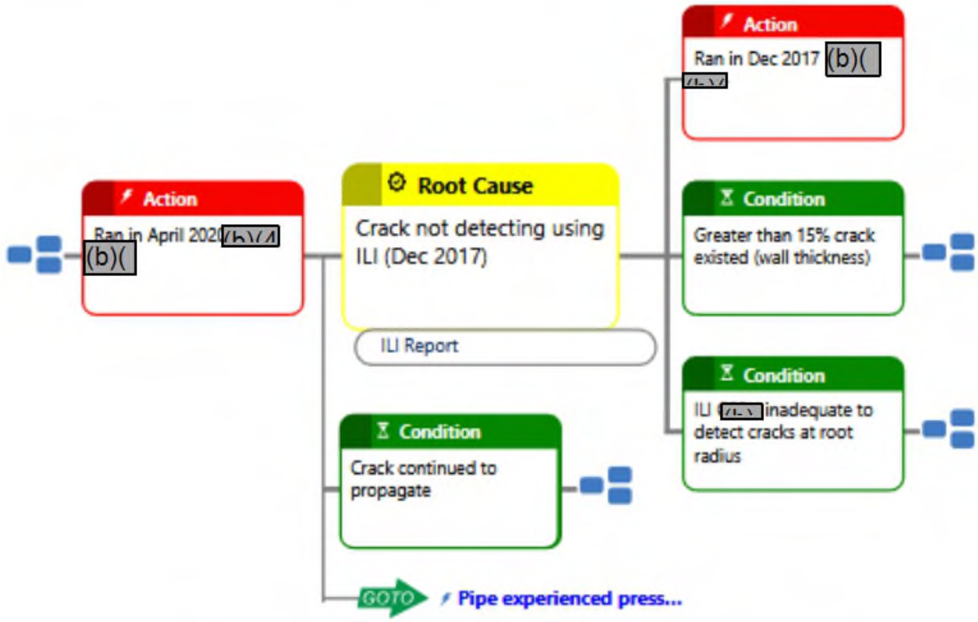

Figure 100: Causes for running the April 2020 (b)(4)

The cause for the crack continuing to propagate is summarized below in Figure 101. The pipe experiences pressure cycles during operations, and the number of cycles continues to decrease over time. Additionally, the presence of hydrogen was likely caused by a minor quantity of water and high TAN diluted bitumen commodities transported; the tar sands environment could have contributed to the formation of hydrogen.

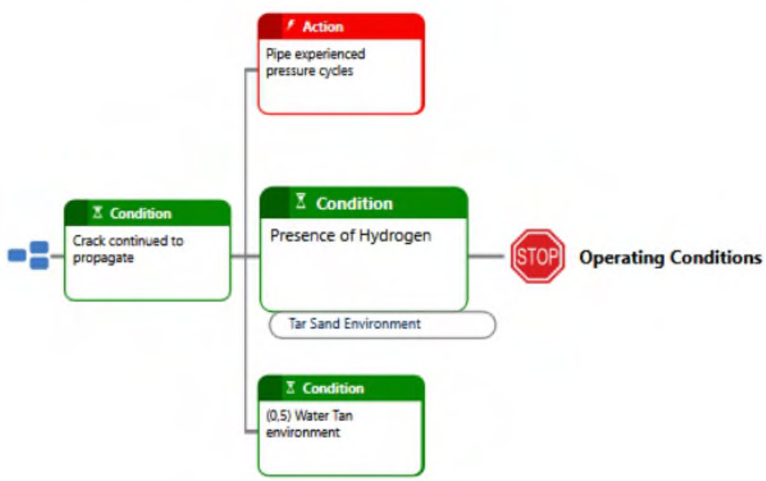

Figure 101: Causes for crack propagation.

The cause for a crack greater than 15% in 2017 is explored below in Figure 102. The reason for this was that the pipeline had been in operation since 2010. Based on modeling and metallurgical data, Blade estimates that a crack of approximately 10-15% existed in 2010. This crack existed in 2010 due to transportation fatigue.

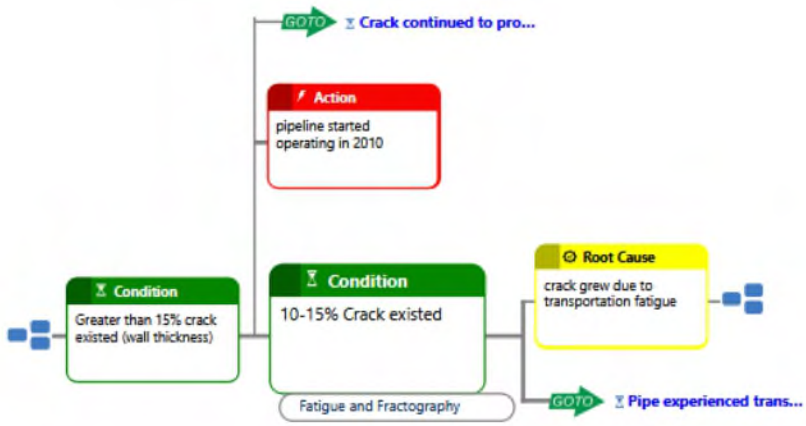

Figure 102: Causes for a crack greater than 15% in 2017

The causes of crack growth through transportation fatigue are described below in Figure 103.

- Crack had to initiate at the weld root radius on the ID during transportation. The initiation was due to a combination of weld geometry and transportation loads. The data indicates that rail transportation was per guidelines, and the weld geometry was also consistent with API specification. However, the presence of the peaking and weld bead offset contributed to high SCF that resulted in crack initiation and growth during transportation.
- There is a high stress concentration at the root radius.
- The Pipe experienced transportation loading cycles. The causes for this include
  - Berg followed the AAR specification of loading pipe.
  - API 5L1 transportation specification existed and was specified by TC Energy. It is important to note that API 5L1 defers to AAR when there is a conflict in guidelines between the documents.

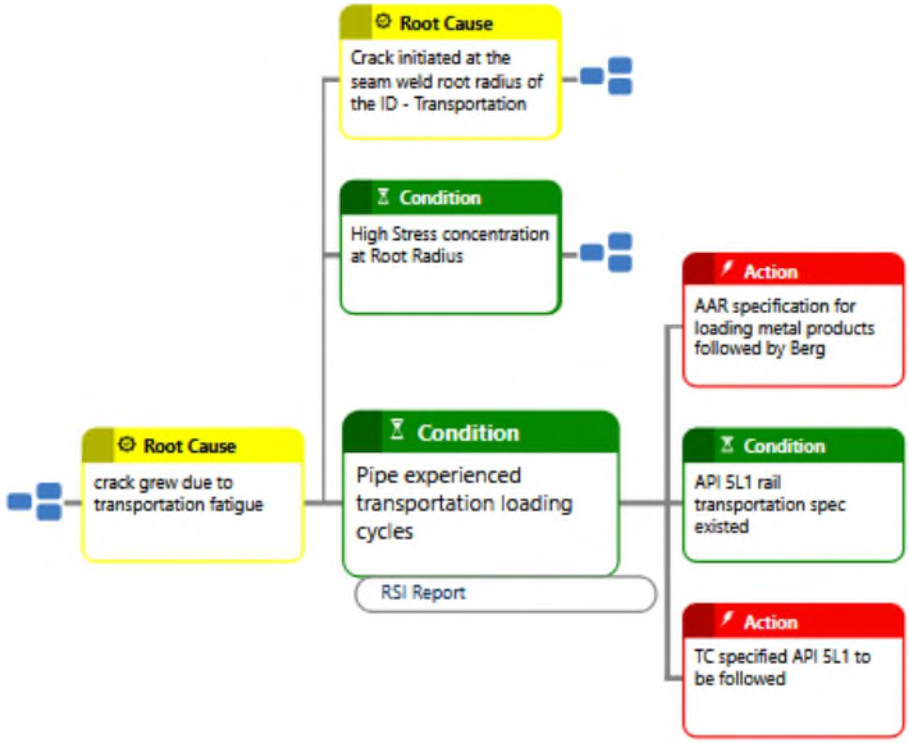

Figure 103: Causes for crack propagation during transportation

The cause of the high stress at the root radius is the weld geometry, specifically a combination of peaking weld geometry and an out-of-line weld, resulting in high SCF at the weld toe. The weld bead is a termination point due to a lack of control.

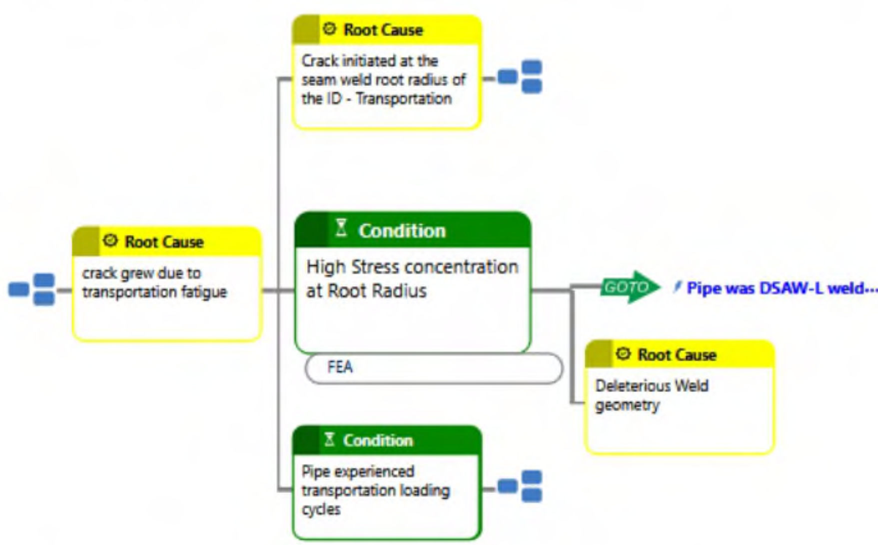

Figure 104: Cause for high stress concentration at the root radius

11.3 Root Causes

Following the evidence-based approach to root cause analysis, the following were identified as the root causes of the failure at MP 171.

1. The weld geometry at MP 171 consists of peaking and weld bead offset; there was almost no plate offset. Depending on the magnitude of these geometric features, even two of these contribute to fatigue susceptibility.
    a. The weld geometry enabled the crack initiation and propagation during transportation, which was primarily on rail. Berg followed the AAR OTLR 2007 guidelines; TC required API 5L1 2004 guidelines. However, API 5L-2004 defers to AAR OTLR 2007 in the event of a conflict. The standard practice, even in 2008, was never to have the seam weld in contact with adjacent pipe joints or dunnage when the pipe was stacked during transportation.
2. The weld geometry conformed to API 5L 43rd edition and TES-PIPE-SAW-US.
3. The successful verification runs for the two UT shear wave technologies provided misplaced confidence in the ability of the UT shear wave tool technology.
4. The inability of the inline crack inspection tools, such as (b)(4) [redacted] (b)(4) [redacted] to detect the crack initiating and propagating in the weld toe. In 2020, TC and (b)(4) [redacted] undertook modeling and full-scale correlation runs to verify the (b)(4) [redacted] for peaked geometries; however, the tool was still unable to identify the crack at MP 171. Notably, the tools didn't exhibit any crack-like signal at the rupture location.
5. Crack initiation and growth during transit with the weld.
6. Fatigue crack propagation during operation is enhanced due to the HAZ microstructure and then further enhanced by hydrogen damage. This is evidenced by the fractographic evidence of the failure, LECO hydrogen measurements, oil modeling, and the J-R curve from the unused pipe that demonstrated HAZ microstructural issues.
7. The internal hydrocarbon environment and pressure cycles are factors in crack propagation; however, South Bow has significantly reduced the cyclic pressure load on the pipeline over time.

11.4 Mitigation and Solutions

The mitigation or solutions necessary to prevent another such weld HAZ crack rupture are summarized below.

1. Improve pipe specifications to account for weld peaking and weld bead offset. QA/QC procedures should be enhanced to locate such welds. In the future, the efficacy of NDE techniques in locating welds (peaking, weld bead offset, and plate offset) should be assessed. If the NDE techniques prove to be inadequate, sectioning certain joints may be necessary to verify weld integrity based on deviation from welding control parameters.
2. The mitigation of the current or possible crack-like anomalies in the pipeline is most critical to ensure rupture prevention. The most efficient way to accomplish this is by using inline inspection tools and technology.

a. Phased Array inline inspection tool technology presents an opportunity to overcome some of the challenges of peaking weld. This represents the best possible solution to prevent such ruptures.

b. South Bow should also evaluate other vendors' UT shear wave tools and assess their weld peaking limitations. Evaluate them with correlation spools and UT simulations.

c. To evaluate all tool technologies, a realistic crack geometry with a realistic weld geometry is necessary to assess the efficacy of the tools.

   i. South Bow should generate the worst-case and realistic weld geometries (similar to the 2020 correlation run). These should be developed from more detailed weld geometry modeling as discussed in Section 5.4.2.

   ii. Then, initiate fatigue cracks either through pressure cycling, like in operations, or by applying external loads.

d. Until a viable crack detection tool is available, it is recommended that a combination of tools/technologies be used to locate regions of the seam weld that exhibit peaking and weld offset. Excavate them and examine with PAUT to identify cracking. An approach similar to the one described below should be considered and further developed.

   i. Identify the weld geometry that might have a pre-existing crack before pipeline operations using the following (or similar) process. Conduct a detailed transit fatigue analysis as a function of weld peaking, plate offset, and weld bead offset. Identify all combinations that may result in crack initiation. This should establish the parameters for the weld geometry that may be susceptible, identified, and perhaps excavated.

   ii. TC/South Bow and (b)(4) have developed a methodology using UT compression waves to locate weld peaking/rooftopping. South Bow has reviewed the UT MP data for the ruptured location and was unable to identify the roof topping. Additional technologies should be integrated with this tool run to improve the effectiveness of this approach.

   iii. Magnetic technologies, such as axial or circumferential MFL, could identify meandering welds. The efficacy of this must be confirmed and verified by South Bow.

   iv. Circumferential MFL should be evaluated for the possibility of identifying these weld cracks. The crack mouth opening displacement (CMOD) will increase due to internal pressure. It may be worth discussing with ILI vendors. They may also be impacted by peaking welds; however, that should be at least qualitatively or quantitatively evaluated and tested.

   v. By combining approaches with UT shear wave data, welds can be identified.

   vi. Then, utilizing the operating pressure and operating pressure cycling severity, the susceptible welds can be identified, excavated, and examined. Blade understands that South Bow has combined UT compression and UT shear wave and identified a crack adjacent to MP 171.

e. If none of the above approaches exhibit efficacy, then hydrostatic testing of similar pipe within the Affected Pipeline needs to be considered. Hydrostatic testing presents several challenges for this pipeline; it could initiate cracks in the weld locations, and if there are subcritical cracks, they would exhibit further tearing. This should be

3. South Bow should quantify crack propagation behavior through the HAZ. This will be important to estimate re-inspection frequency.
    a. Characterize the HAZ microstructure in the peaked weld and the standard weld. This should be conducted with EBSD and other advanced characterization methods.
    b. Conduct fracture toughness testing at operating temperatures, and assess the fracture surface for cleavage indications.
    c. Evaluate crack initiation through the HAZ and compare it with base metal using notched specimens.
    d. Characterize FCGR through HAZ and compare it with previous testing in air.
    e. Characterize FCGR through HAZ in an electrochemical hydrogen environment. Quantify the rates and use this to assess crack growth. The testing should be evaluated with increasing hydrogen quantity to evaluate the impact on fractography.

11.5 Summary – Root Causes and Mitigation

Table 22: Summary of RCAs and solutions

Root Causes	Solutions
Seam Weld – A Combination of Peaking and Weld Bead Offset (Section	Enhanced pipe manufacturing standards and QA/QC to prevent welds.
Specifications are inadequate to locate weld peaking and weld bead offset.	
Successful verification runs that resulted in misplaced confidence in the UT shear wave technology.	Create a verification spool that features peaking welds, bead offsets, and tilted fatigue cracks.
The inability of multiple UT shear wave tools to detect this anomaly.	• Since POD is low for the current crack ILI technologies, locate, verify, and mitigate all crack-like signals. • Phased array ILI technology requires evaluation for crack detection. • A combination of ILI technologies, such as UT Compression wave, along with other factors such as pressure and cyclic loads, is used to identify peaking welds. • Assess magnetic technologies to evaluate their ability to detect cracks and also perhaps geometric anomalies in welds. • If none of the above tools exhibit efficacy, consider hydrostatic testing as an alternative. Such a test is fraught with issues, including the initiation of cracks at weld toes and the exacerbation of subcritical cracks.

Root Causes	Solutions
Crack initiated and propagated during transit.	Enhanced QA/QC and pipe manufacturing standards to prevent weld peaking and bead offset.
Crack propagation during oil transportation was further enhanced by hydrogen and HAZ microstructure.	HAZ microstructure characterization, followed by crack initiation and propagation behavior characterization in a hydrogen environment, to establish a re-inspection frequency.
The internal oil environment contributed hydrogen and cyclic pressure loads.	South Bow has already minimized cyclic loads, and this is an operational reality.

12 References

[1] Anderson and Associates Inc., "Metallurgical Analysis of 30in Keystone Phase 1 Pipeline Rupture," Anderson and Associates, Houston, 2019.

[2] Anderson and Associates, Inc., "Metallurgical Analysis of NPS-30 MP-171 Pipeline Incident," Anderson and Associates, Houston, 2025.

[3] American Petroleum Institute, *API 5L Specification for Line Pipe,* American Petroleum Institute, 2004.

[4] *Keystone Oil Pipeline Project US Pipeline Construction Construction Contract No. 5180,* TransCanada, 2007.

[5] Berg Steel Pipe Corp, *MPS - BSPC - TC- 03 Rev1 Manufacturing Procedure Specification,* Berg Steel Pipe Corp.

[6] American Petroleum Institute, *Welding of Pipelines and Related Facilities,* 2005.

[7] Y. Dong and et al, "Correlation between Microstructure and Mechanical Properties of Welded Joint of Submarine Pipeline Steel with Heavy Wall Thickness," *metals,* vol. 12, no. 716, 2022.

[8] E. S. Drexler, A. J. Slifka, R. L. Amaro, J. W. Sowards, M. J. Connolly, M. L. Martin and D. S. Lauria, "Fatigue Testing of Pipeline Welds and Heat-Affected Zones in Pressurized Hydrogen Gas," *Journal of Research of the National Institute of Standards and Technology,* vol. 124, no. 124008, 2019.

[9] H. Yu and et al, "Effect of Heat-Input on Microstructure and Toughness of CGHAZ in a High-Nb-Content Microalloyed HSLA Steel," *Materials,* vol. 15, no. 3588, 2022.

[10] Z. Zhao, P. Xu, H. Cheng, J. Miao and F. Xiao, "Characterization of Microstructures and Fatigue Properties for Dual-Phase Pipeline Steels by Gleeble Simulation of Heat-Affected Zone," *materials,* 20 June 2019.

[11] C. R. Roper, "A Study of the Factors Influencing Transition Temperature of A537," Bethlehem, 1967.

[12] R. O. Ritchie and J. F. Knott, "Micro Cleavage Cracking During Fatigue Crack Propagation in Low Strength Steel," *Material Science and Engineering,* vol. 14, 1974.

[13] ASTM International, *ASTM E1820-24 Test Method for Linear-Elastic Plane-Strain Fracture Toughness of Metallic Materials,* Conshohocken: ASTM International, 2024.

[14] ASTM International, *ASTM E399-24 Linear-Elastic Plane-Strain Fracture Toughness KIc of Metallic Materials,* Conshohocken: ASTM International, 2024.

[15] R. I. Stephens, A. Fatemi, R. R. Stephens and H. O. Fuchs, Metal Fatigue in Engineering, Wiley-Interscience, 2000.

[16] American Petroleum Institute, *API 579-1/ASME FFS-1 Fitness-For-Service,* Washington, DC: American Petroleum Institute, 2021.

[17] Anderson & Associates, Inc., "250145 South Bow - Metallurgical Analysis of NPS-30 MP-171 Pipeline Incident," 2025.

[18] R. P. Gangloff and R. G. Kelly, "Microbe-Enhanced Environmental Fatigue Crack Propagation in HY130 Steel," *Corrosion Science,* vol. 50, pp. 345-354, 1994.

[19] B. Zand, "Keystone Seam Finite Element Analysis and Transit Fatigue Assessment," RSI Pipeline Solutions, New Albany, Ohio, 2020.

[20] N. E. Dowling, "Mean Stress Effects in Stress-Life and Strain Life Fatigue," in *Paper F2004/51*, 2004.

[21] Berg Steel Pipe Corp., *BPP-SOP-MQC-002,* Panama City: Berg Steel Pipe Corp, 2019.

[22] South Bow, "TEN - MP 171 Loss of Containment Analysis," 2025.

[23] U.S. Department of Transportation, Pipeline and Hazardous Materials Safety Administration, Hazardous Liquid Accident Data - January 2010 to present, 2025.

[24] South Bow, "LPCC - Leak Detection System, Version 2.0.0," 2025.

[25] South Bow, "ICS Form 202 - Incident Objectives MP 171," 2025.

[26] TC Energy, "Keystone Pipeline System Emergency Response Plan (CAN-US), Rev. 10, Item ID# 009213528," 2024.

[27] RSI Pipeline Solutions, "Root Cause Failure Analysis for the Keystone Pipeline Edinburg +0.2 Release," 2000.

[28] G. Bakker, "The Corrosive Nature of Diluted Bitumen and Crude Oil Literature Review," M. R. Gordon and Associates, 2011.

[29] J. Zhou and J. Been, "Comparison of the Corrosivity of Dilbit and Conventional Crude," *Alberta Innovates - Technology Futures,* September 2011.

[30] G. W. Bruce, "Bitumen to Finished Products," in *Canadian Heavy Oil Association Technical Luncheon*, Calgary, 2005.

[31] W. Wang and A. Watkinson, "Iron Sulphide and Coke Fouling from Sour Oils Review and Initial Experiments," in *Proceedings of the International Conference on Heat Exchanger*, 2011.

[32] M. R. Gray, "Upgrading Petroleum Residues and Heavy Oils," Marcel Dekker, 1994.

[33] J. F. Moulder, W. F. Stickle, P. E. Sobol and K. D. Bomben, Handbook of X-ray Photoelectron Spectroscopy, Physical Electronics, Inc, 1995.

[34] A. Y. Lee, "NIST X-Ray Photoelectron Spectroscopy Database, Ver 4.1," Gaithersburg, 2012.

[35] A. P. Grosvenor, B. A. Kobe, M. C. Biesinger and N. S. McIntyre, "Investigation of multiplet splitting of Fe 2p XPS spectra and bonding in iron compounds," *SURFACE AND INTERFACE ANALYSIS,* pp. 1564-1574, 7 October 2004.

[36] T. Yamashita and P. Hayes, "Analysis of XPS spectra of Fe2+ and Fe3+ ions in oxide materials," *Applied Surface Science,* vol. 254, 2008.

[37] P. S. Bagus, C. J. Nelin, C. R. Brundle, B. V. Crist, N. Lahiri and K. M. Rosso, "Combined Multiplet Theory and Experiment for the Fe 2p and 3p XPS of FeO and Fe2O3," *The Journal of Chemical Physics,* 3 March 2021.

[38] ThermoFisher, "Iron X-ray photoelectron spectra, iron electron configuration, and other elemental information," 2025.

[39] *TES- PIPE - SAW-US specification for SAW pipe, Rev 0, Dec 7 2006.*

[40] American Petroleum Institute, *API 5L1 Recommended Practice for Railroad Transportation of Line Pipe,* 6 ed., Washington, DC: API, 2002.

[41] TC Energy, *PPA -5165 - 5590 Purchase Agreement,* Calgary, AB, Canada: TransCanada.

[42] American Petroleum Institute, *API 5L Specification for Line Pipe,* 44 ed., Washington, DC: API, 2008.

[43] American Petroleum Institute, *API 5L Specification for Line Pipe,* 46 ed., Washington, DC: API, 2018.

[44] TC Energy, *DMP ENC V-08-32 Manufacturing Surveillance,* TC Energy.

[45] *MTR -NPS30-386.*

[46] Berg Steel Pipe Corp., *BPP-SOP-SHP-005 Rail Car Banding Procedure,* Berg Steel Pipe Corp..

[47] *AAR open top loading rules manual, section 2, Part3, Dec 2007.*

[48] American Petroleum Institute, *API 5LT Recommended Practice for Truck Transportation,* Washington, DC: API, 2019.

[49] D. L. Gano, RealityCharting - Seven Steps To Effective Problem-Solving and Strategies for Personal Success, Richland, Washington: Apollonian Publications, 2011.

[50] Berg Steel Pipe Corp., "SAWL (3RB) Manufacturing Process," [Online]. Available: https://www.borusanbergpipe.com/3rb-manufacturing-process. [Accessed 15 07 2025].

Appendix A Apollo RCA Results

(b)(4)